MULTI-CHANNEL BLIND SYSTEM IDENTIFICATION USING THE LAGUERRE EXPANSION FOR CHARACTERIZATION OF CIRCULATORY HEMODYNAMICS

by

DEVIN BARNETT MCCOMBIE

B.S., Bioengineering
University of California, San Diego, 2000

Submitted to the Department of Mechanical Engineering and the
Department of Electrical Engineering and Computer Science
in Partial Fulfillment of the Requirements for the Degrees of

Master of Science in Mechanical Engineering
and
Master of Science in Electrical Engineering and Computer Science

at the
Massachusetts Institute of Technology
June 2004

Signature of Author_____
Department of Mechanical Engineering
May 13, 2004

Certified By_____
H. Harry Asada
Ford Professor of Mechanical Engineering
Thesis Supervisor

Accepted by_____
Ain A. Sonin
Chairman, Department Committee on Graduate Students
Department of Mechanical Engineering

Accepted by_____
Arthur C. Smith
Chairman, Department Committee on Graduate Students
Department of Electrical Engineering and Computer Science

MULTI-CHANNEL BLIND SYSTEM IDENTIFICATION USING THE LAGUERRE EXPANSION FOR CHARACTERIAZATION OF CIRCULATORY HEMODYNAMICS

by

DEVIN BARNETT MCCOMBIE

Submitted to the Department of Mechanical Engineering and the
Department of Electrical Engineering and Computer Science
On May 13, 2004 in partial fulfillment of the requirements
for the Degree of Master of Science in Mechanical Engineering
and for the Degree of Master of Science in Electrical Engineering
and Computer Science

ABSTRACT

A new tool for real-time characterization of both systemic and local circulatory hemodynamics has been developed. Given two peripheral circulatory waveform measurements this new signal-processing algorithm generates two low order models that represent the distinct branch dynamic behavior associated with the measured circulatory signals. The framework for this methodology is based on a multi-channel blind system identification technique that has been reformulated to use a Laguerre basis function series expansion. The truncated Laguerre series expansion allows a highly compact representation of the cardiovascular dynamics. This new algorithm has been applied to experimental arterial blood pressure measurements derived from a swine model and shown to consistently provide accurate identification of the vascular hemodynamics.

The parameters of the circulatory dynamics that are quantified in real-time via this newly developed algorithm, Laguerre Model Blind System Identification (LaMBSI), can be used to identify or quantify systemic and local cardiovascular features of interest. The LaMBSI algorithm identifies a set of six parameters per channel when applied to measured circulatory signals, 5 distinct model coefficients plus 1 common Laguerre basis pole shared by both channels. The two sets of identified parameters can be treated as feature vectors and standard statistical techniques can be used to extract information from this compact time series of data. In this thesis, a multi-parameter linear regression is used to predict cardiac output based on the LaMBSI feature vectors identified from two pulsatile arterial pressure signals. The promising results from this linear regression model serves as a proof-of-principle that the hemodynamic parameters identified from two distinct circulatory waveform signals using the LaMBSI algorithm can be used to characterize systemic or global parameters within the circulatory system.

Thesis Supervisor: H. Harry Asada
Title: Ford Professor of Mechanical Engineering

Acknowledgments

The completion of this thesis would not have been possible without the contributions of the following people.
Professor H. Harry Asada my thesis advisor, whose guidance and instruction served as the cornerstones for this work and who fostered my personal growth and development as a researcher and engineer.
Dr. Andrew Reisner who collaborated with me on this research and whose knowledge of medicine and cardiovascular monitoring provided me with numerous insights and inspiration, and who contributed the detailed description of the animal experiment protocol.
All the students of the d'Lab both past and present who made those long hours a little easier and who offered me a friendly ear when I needed it.

Most importantly, I would like to thank my wife, Lisa, who has been my greatest source of inspiration and whose support has carried me through all those long weeks and late nights. I am truly blessed to have you in my life.

I would also like to thank my family for their support throughout the years, no matter what path I followed they were always there for me.

I dedicate this thesis in memory of my grandparents, Ben and Vivian, who showed me both the value of hard work and the importance of always making room for laughter in our lives.

Table of Contents

List of Figures

1. Introduction

1.1 Impediments to Circulatory Waveform Analysis

It is a challenge to characterize blood flow in the human circulatory system. The arborizing network of blood vessels emanating from the heart creates a system that exhibits both lumped and distributed fluid dynamic behavior. Additionally, the circulatory system possesses a time varying attribute that further increases the complexity of the structure. Given this framework it is difficult to reliably quantify cardiovascular parameters using standard analytic techniques on measured circulatory waveforms.

A major source of error in quantifying these parameters results from an inability to separate local from systemic phenomenon in the measured waveform signal. This problem is amplified when monitoring patients that experience fluctuations in their cardiovascular state. For instance, pressure and flow relationships for any arterial branch are complicated by the superposition of antegrade and retrograde pressure waves. This is one source of error in many of the well-known techniques for estimating cardiac output from a single arterial pressure waveform [9-12]. The measured waveform signal in one location can also be altered by local flow phenomena in distant locations, regardless of the systemic hemodynamic state. For instance, blood moves from the lower extremities into the renal arteries late in diastole whereas an occlusion in the renal arteries eliminates that lower extremity retrograde flow [2].

Alone, a single circulatory measurement cannot uniquely characterize the entire system. It is intuitive that comparing information from additional circulatory signals taken from multiple locations could reveal some branch specific circulatory features while still capturing information on systemic behavior. Conscious of the type of complexity manifested in the cardiovascular system, we have hypothesized, that using additional waveform measurements taken from different anatomic locations and/or using an additional measurement modality can improve our

ability to accurately characterize the cardiovascular system. Taken to its extreme, if hydrodynamic data (e.g. trends in pressure, flow and plethysmograph) were available from every single location of the vascular system, it would be perfectly characterized. This extreme scenario is neither feasible nor useful for any real-world application, but it illustrates the principle that additional measurements should, in theory, offer the means to interpret otherwise ambiguous features in the waveform measurements.

Therefore, we have developed a general methodology for comparing multiple circulatory signals in order to accurately characterize the cardiovascular system. A signal-processing algorithm taken from wireless communications called Multi-channel Blind System I.D. provides the framework for this methodology.

1.2 A Multi-Channel View of the Cardiovascular System

A wireless communication system can be used to illustrate the salient features of a multi-channel dynamic system. In this system a common broadcast signal is transmitted across different paths that individually modify the source signal, which is then received simultaneously by multiple receivers. The cardiovascular system is topologically analogous to a multi-channel dynamic system. A common flow input originates from the heart and produces pressure waves that are broadcast and transmitted down multiple vascular pathways or channels to distinct measurement sites. Multiple sensors placed at different locations on the patient will yield simultaneous circulatory signals. These measurements can be treated as multi-channel data and processed with a multi-channel blind system identification algorithm.

Our new technique for comparing measured circulatory signals is dependent upon the multi-channel structure of the cardiovascular system. This new cardiovascular monitoring tool, Laguerre Model Blind System Identification (LaMBSI), identifies a compact quantitative

description of both the local and systemic hemodynamic behavior in the measured signals in real-time.

We have hypothesized that the distinct cardiovascular dynamics that are identifiable given two appropriately selected circulatory waveforms and parameterized via LMBSI, can identify or quantify circulatory phenomena of interest, including both systemic (global) hydrodynamic phenomena and branch specific (local) hydrodynamic phenomena. This might enable the estimation of the vascular resistance of a single artery, or the total peripheral resistance (TPR), assuming the LaMBSI terms correlate with the physiologic parameters of interest. Similarly, the technique may permit the identification of local vascular pathology (such as stenosis in an extremity or renal artery) or quantification of a global arterial parameter such as total compliance.

1.3 Past Advances in Cardiovascular Blind System Identification

Previous efforts have been made to apply Multi-Channel Blind System Identification (MBSI) to measured circulatory waveform signals [1]. However, existing MBSI theory is not directly applicable to the cardiovascular system, and earlier attempts using the traditional techniques have revealed several shortcomings.

- The method requires co-prime channels, but the dynamics of the arterial network are not co-prime, containing common poles that result from all channels initially traveling a common path.
- Models representing the complex cardiovascular dynamics tend to be of high order, placing too large a demand on the uncontrolled input in order to meet the necessary persistence of excitation requirements.

- Blind system identification using a standard auto-regressive moving average (ARMA) model requires at least three distinct sensor measurements, this is difficult to accommodate in a clinical setting or with wearable sensors given the anatomy of the arterial system.

The first limitation has been removed with a new method that identifies the distinct part of the channel dynamics separately from the common dynamics [1].

1.4 Summary and Organization

In this paper we describe an improved blind system identification methodology that has been adapted specifically to the cardiovascular system. In contrast to the previous algorithm it can perform using just two distinct circulatory signals and provides a more compact, lower-order model to quantify the circulatory parameters. Results from applying this new algorithm to pressure measurements derived from a swine model will show that LaMBSI consistently identifies the hemodynamics with good accuracy and that the identified parameters reveal both local and systemic cardiovascular features.

Additionally, this paper offers an initial proof-of-principle that the parameters identified using LaMBSI can be used to estimate a physiologic parameter of interest, namely TPR. In this investigation, the technique was used on two distinct arterial blood pressure (ABP) waveforms obtained in a swine model. ABP's were selected because (a) the experimentalists had extensive familiarity with this instrumentation; (b) computer models are available for theoretical exploration of the relationship between global hemodynamics and pressure within individual models; (c) the relatively direct relationship between pressure and flow in the CV system, and (d) although there are many existing techniques which estimate CO from a single ABP signal, most fail to account for retrograde pressure waves leading to a source of error and opportunity for

improvement. In future work, the estimation of hemodynamics using LaMBSI with less invasive hydrodynamic signals will be investigated, because twin ABP measurements may not always be feasible in clinical settings.

2. Laguerre Model Blind System Identification

2.1 The Multi-Channel Blind System Cross Relation

A brief review of the MBSI algorithm can be explained by considering a linear multi-channel dynamic system consisting of two distinct channels connected to the same input, as shown in Figure 1.

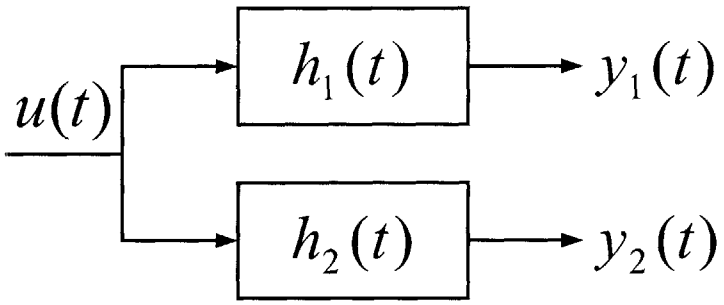

Figure 1: Block diagram of a two-channel system

Both of the observed outputs, $y_1(t)$ and $y_2(t)$ are excited by a common input $u(t)$, and can be represented as the convolution of this input and the corresponding channel impulse responses.

$$y_1(t) = h_1(t) * u(t) \quad \text{and} \quad y_2(t) = h_2(t) * u(t) \tag{1}$$

Given this type of multi-channel system, having an unknown input signal $u(t)$ we want to determine both the channel dynamics, i.e. impulse response functions $h_1(t)$ and $h_2(t)$, and the common input using only the measured outputs $y_1(t)$ and $y_2(t)$. It is generally impossible to perform this identification if only one output is observed however utilizing the inherent

relationships between the two channels and measured outputs the problem can be solved. Consider the formula shown in equation 2.

$$y_1(t) = h_1(t) * u(t) \tag{2}$$

Both sides of this equation defining the relationship between the input and output of channel 1 can be convolved with the impulse response of channel 2, $h_2(t)$.

$$h_2 * y_1(t) = h_2(t) * \left(h_1(t) * u(t)\right) \tag{3}$$

Applying the associative law for linear convolution this equation can be rewritten:

$$h_2 * y_1(t) = h_1(t) * \left(h_2(t) * u(t)\right) \tag{4}$$

The terms in parentheses can be replaced given the previous definition in equation 1 describing the output of channel 2. Therefore the correlation between the outputs of the two channels can be represented by the equality shown in equation 5.

$$h_2(t) * y_1(t) = h_1(t) * y_2(t) \tag{5}$$

Note that this correlation equation does not include input $u(t)$. Therefore, although the input cannot be measured, this equation can still be formulated.

2.2 Standard Delay Expansion Blind System Identification

The impulse response of a causal system can be represented using a series expansion as shown in equation 6. This expansion consists of a set of orthonormal basis functions, $\{V_k(z)\}_{k=0,1,2,\ldots}$ and real valued expansion coefficients, $\{b_k\}_{k=0,1,2,\ldots}$.

$$H(z) = \sum_{k=0}^{\infty} b_k V_k(z) \tag{6}$$

In practice, a model representation is implemented by approximating the system's impulse response using a finite series expansion, or finite impulse response (FIR) model.

$$\hat{H}(z) = \sum_{k=0}^{L-1} b_k V_k(z) \tag{7}$$

Utilizing the standard delay operator basis function, $V_k(z) = z^{-k}$, the transfer function representing the impulse response of a dynamic system is described using the approximation shown in equation 8.

$$\hat{H}(z) = \sum_{k=0}^{L-1} b_k z^{-k} \tag{8}$$

This familiar model can be used in the MBSI equality described above to develop a system of simultaneous equations to solve for the unknown expansion coefficients [3]. For example, in a two-channel system the impulse responses of each channel can be represented using the delay operator expansion.

$$\hat{H}_1(z) = \sum_{k=0}^{L_1-1} b_k^1 z^{-k} \text{ and } \hat{H}_2(z) = \sum_{k=0}^{L_2-1} b_k^2 z^{-k} \tag{9}$$

Therefore the MBSI equality that correlates the outputs of the two channels will assume the following form.

$$\left(\sum_{k=0}^{L_2-1} b_k^2 z^{-k} \right) y_1(t) = \left(\sum_{k=0}^{L_1-1} b_k^1 z^{-k} \right) y_2(t) \tag{10}$$

For a given time series of observed outputs, we can formulate simultaneous equations containing the unknown expansion coefficients.

$$\left(b_0^2 y_1(t) + b_1^2 y_1(t-1) + \ldots + b_{L_2-1}^2 y_1(t-(L_2-1))\right) -$$

$$\left(b_0^1 y_2(t) + b_1^1 y_2(t-1) + \ldots + b_{L_1-1}^1 y_2(t-(L_1-1))\right) = 0 \tag{11}$$

This correlation can be formulated into a matrix equation (eqn. 12) given a time series of data to form an over constrained set of linear equations with the number of data samples, $N > L_1 + L_2$, and a data time sequence with final time, $t > N+L$ where L is equal to the larger value of L_1 or L_2.

$$\begin{bmatrix} y_1(t-N-L_2-1) & \cdots & y_1(t-N) \\ \vdots & & \vdots \\ y_1(t-L_2-1) & \cdots & y_1(t) \end{bmatrix} \begin{bmatrix} b_{L_2-1}^2 \\ \vdots \\ b_0^2 \end{bmatrix} -$$

$$\begin{bmatrix} y_2(t-N-L_1-1) & \cdots & y_2(t-N) \\ \vdots & & \vdots \\ y_2(t-L_1-1) & \cdots & y_2(t) \end{bmatrix} \begin{bmatrix} b_{L_1-1}^1 \\ \vdots \\ b_0^1 \end{bmatrix} = \begin{bmatrix} 0 \\ \vdots \\ 0 \end{bmatrix} \tag{12}$$

The equality of equation 12 can be written using a more compact representation for the matrices, $Y_1 H_2 - Y_2 H_1 = 0$, and then all the terms arranged into a single matrix.

$$\begin{bmatrix} Y_1 & -Y_2 \end{bmatrix} \begin{bmatrix} H_2 \\ H_1 \end{bmatrix} = 0 \tag{13}$$

Under certain specified identifiably conditions, i.e. conditions needed for uniquely determining the transfer functions from output data alone [3,4], this set of simultaneous equations can be solved for the unknown parameters of the two impulse response functions using a technique such as single value decomposition. Once the channel dynamics are determined, then the input can be recovered from the outputs and the identified channel dynamics by filtering the measured outputs through an appropriate inverse filter.

2.3 Laguerre Expansion Blind System Identification

The number of expansion coefficients required in a truncated series expansion to accurately model the impulse response of a system depends on the process dynamics, the data-sampling rate, and type of basis expansion functions. If the system exhibits a slow decaying impulse response, because of a pole on or near the unit circle, the standard delay operator expansion function, $V_k(z) = z^{-k}$, will require a large number of coefficients to accurately represent the system dynamics.

In the context of a system identification problem the requirement for a large number of expansion coefficients places a high demand on the system input in order to meet the necessary persistence of excitation conditions to uniquely identify them within the model set [5].

The required number of expansion coefficients needed to accurately represent the system's impulse response can be significantly reduced if an appropriate set of basis function expansions are used that incorporate *a priori* knowledge of the system's dynamic response.

Various classes of orthonormal basis functions have been proposed to model the impulse response of systems with slow decaying dynamics [5][7][8], one predominant type is a class known as Laguerre functions.

The general form of the Laguerre expansion function is shown below (eqn. 14) where the parameter a, in this function represents an estimated value of the dominant slow decaying system pole.

$$V_k(z) = \frac{K}{(z-a)}\left(\frac{1-az}{z-a}\right)^{k-1} \text{ ; with } K = \sqrt{(1-a^2)T} \tag{14}$$

Using Laguerre basis functions, a new type of FIR model can be formulated to approximate the impulse response of a dynamic system.

$$\hat{H}(z) = \sum_{k=1}^{L} b_k \frac{K}{(z-a)} \left(\frac{1-az}{z-a} \right)^{k-1} \tag{15}$$

The predicted output of a dynamic system can be written using the Laguerre FIR model as a linear regression involving the current input and past values of the input and output.

$$y(t) = \left(\sum_{k=1}^{L} b_k \frac{K}{(z-a)} \left(\frac{1-az}{z-a} \right)^{k-1} \right) u(t) \tag{16}$$

The Laguerre FIR model can be represented using a filter bank that consists of functions written in terms of the Z-transform operator as shown in figure 2.

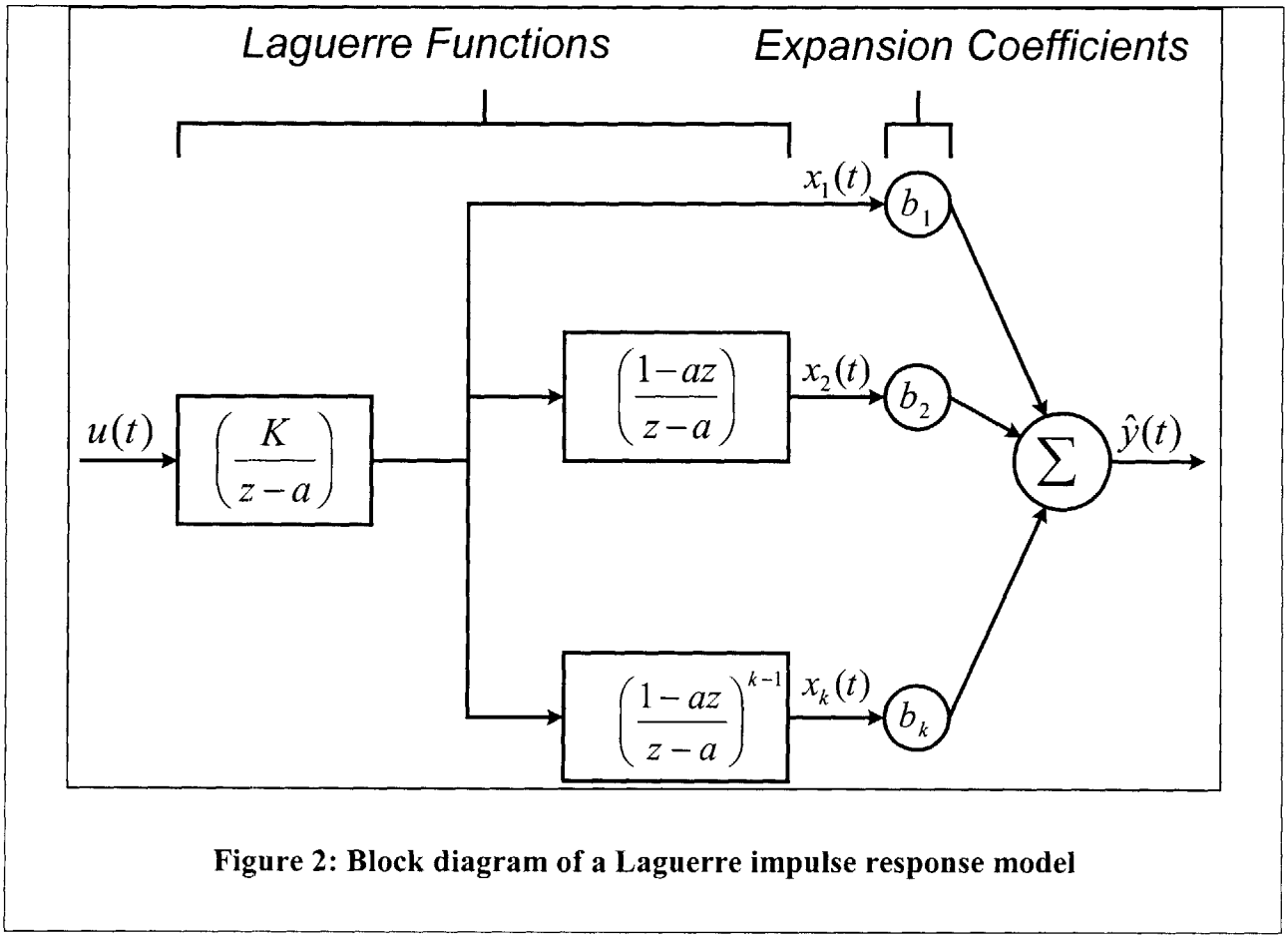

Figure 2: Block diagram of a Laguerre impulse response model

Thus, implementation of a Laguerre model can be viewed as pre-filtering the input through an appropriate number of Laguerre filters to obtain a transformed set of intermediate variables, $x_i(t)$, which are multiplied by their respective expansion coefficient and summed to obtain the predicted output .

$$y(t) = \sum_{k=1}^{L} b_k x_k(t) \tag{17}$$

This pre-filtering can be implemented in an efficient recursive manner.

$$x_i(t) = \left(\frac{1-az}{z-a}\right) x_{i-1}(t) \tag{18}$$

A direct consequence of using Laguerre models in a system identification problem is that the intermediate variables, $x_i(t)$ can only be implemented once the pre-filtered input has reached its steady state values. Therefore, either some initial conditions must be incorporated into the filtering process or initial transient data points must be disregarded.

Using Laguerre FIR models the individual impulse responses in a two-channel dynamic system can be written as shown in equation 19.

$$\hat{H}_1(z) = \sum_{k=1}^{L_1} b_k^{(1)} \frac{K}{(z-a)}\left(\frac{1-az}{z-a}\right)^{k-1} \text{ and } \hat{H}_2(z) = \sum_{k=1}^{L_2} b_k^{(2)} \frac{K}{(z-a)}\left(\frac{1-az}{z-a}\right)^{k-1} \tag{19}$$

The basic MBSI relationship or equality that correlates the outputs of the two channels in this multi-channel system can be rewritten using these new Laguerre models.

$$\left(\sum_{k=1}^{L_2} b_k^{(2)} \frac{K}{(z-a)}\left(\frac{1-az}{z-a}\right)^{k-1}\right) y_1(t) = \left(\sum_{k=1}^{L_1} b_k^{(1)} \frac{K}{(z-a)}\left(\frac{1-az}{z-a}\right)^{k-1}\right) y_2(t) \tag{20}$$

A block diagram representation of this equality is depicted in Figure 3 using filter banks to represent the finite impulse response series expansions of the two Laguerre models.

The basic MBSI equality relating the two channels can be further simplified by writing it in terms of the Laguerre function pre-filtered output data along with the corresponding expansion coefficients (eqn. 21).

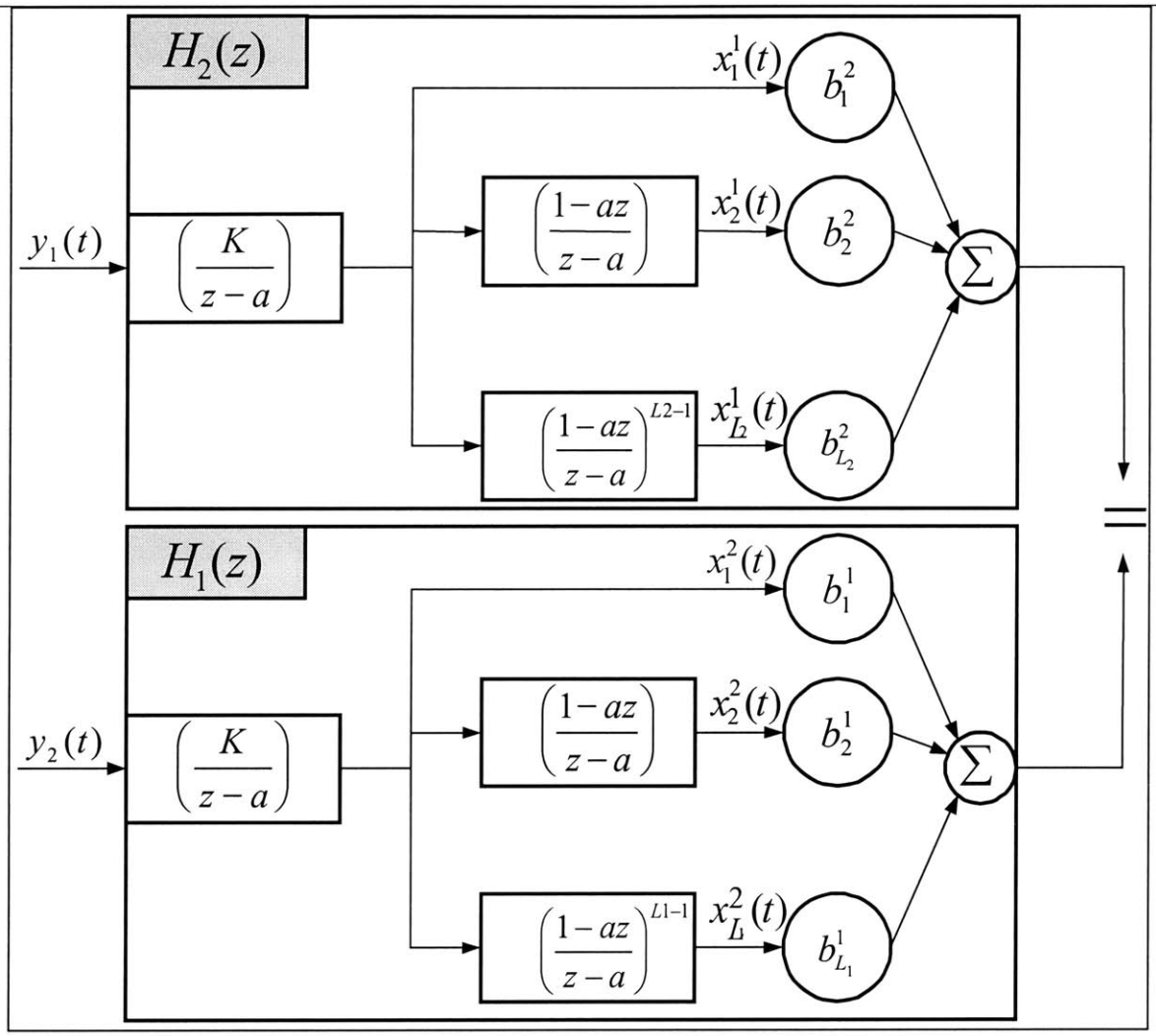

Figure 3: Block diagram of the two channel MBSI equality with Laguerre models

$$\sum_{k=1}^{L_2} b_k^{(2)} x_k^{(1)}(t) = \sum_{k=1}^{L_1} b_k^{(1)} x_k^{(2)}(t) \tag{21}$$

Thus, in contrast to the standard delay operator series expansion models, the filtered intermediate variables, $x_i(t)$, for a given time series of observed outputs are used to formulate simultaneous equations containing the unknown expansion coefficients.

$$b_1^{(2)} x_1^{(1)}(t) + b_2^{(2)} x_2^{(1)}(t) + \cdots + b_{L_2}^{(2)} x_{L_2}^{(1)}(t) = b_1^{(1)} x_1^{(2)}(t) + b_2^{(1)} x_2^{(2)}(t) + \cdots + b_{L_1}^{(1)} x_{L_1}^{(2)}(t) \tag{22}$$

Again, this correlation can be formulated into a matrix equation given a time series of data to form an over constrained set of linear equations such that the number of filtered data samples, $N > L_1+L_2$. And, assuming that for a given time, $t_i = t\text{-}N$, the filtered intermediate variables have achieved their steady state values.

$$\begin{bmatrix} x_1^{(1)}(t) & \cdots & x_{L_2}^{(1)}(t) \\ \vdots & & \vdots \\ x_1^{(1)}(t-N) & \cdots & x_{L_2}^{(1)}(t-N) \end{bmatrix} \begin{bmatrix} b_1^{(2)} \\ \vdots \\ b_{L_2}^{(2)} \end{bmatrix} - \begin{bmatrix} x_1^{(2)}(t) & \cdots & x_{L_1}^{(2)}(t) \\ \vdots & & \vdots \\ x_1^{(2)}(t-N) & \cdots & x_{L_1}^{(2)}(t-N) \end{bmatrix} \begin{bmatrix} b_1^{(1)} \\ \vdots \\ b_{L_1}^{(1)} \end{bmatrix} = \begin{bmatrix} 0 \\ \vdots \\ 0 \end{bmatrix} \tag{23}$$

The matrix equality of equation 23 can be written using a more compact representation for the matrices, $X_1 H_2 - X_2 H_1 = 0$, and then all the terms arranged into a single matrix.

$$\begin{bmatrix} X_1 & -X_2 \end{bmatrix} \begin{bmatrix} H_2 \\ H_1 \end{bmatrix} = 0 \tag{24}$$

Under certain specified identifiably conditions this set of simultaneous equations can be solved for the unknown parameters of the two impulse response functions using single value decomposition.

$$\begin{bmatrix} X_1 & -X_2 \end{bmatrix} = \begin{bmatrix} U \end{bmatrix} \begin{bmatrix} S \end{bmatrix} \begin{bmatrix} V^T \end{bmatrix} \tag{25}$$

Where the right most column vector of the unitary matrix V^T, corresponds to the smallest singular value in the diagonal matrix S, this column vector is considered equivalent to the null space of the data matrix, $[X_1 \quad -X_2]$ and is therefore taken as the estimated value of the expansion coefficient vector.

2.4 Laguerre Model Deconvolution

Deconvolution of the measured outputs to obtain the common input signal using the identified Laguerre system models can be accomplished with an innovative inverse filtering algorithm similar to that proposed by Gurelli and Nikias [4]. This algorithm does not require the identified models to be inversely stable by generating only inverse FIR model filters.

Two Laguerre function impulse response models with identified expansion coefficients $\{b_k^i\}_{k=0,1,2,\ldots}$ can be defined as $H_1(z)$ and $H_2(z)$.

$$H_1(z) = \sum_{k=1}^{L_1} b_k^{(1)} \left(\frac{K}{z-a}\right)\left(\frac{1-az}{z-a}\right)^k \tag{26}$$

$$H_2(z) = \sum_{k=1}^{L_2} b_k^{(2)} \left(\frac{K}{z-a}\right)\left(\frac{1-az}{z-a}\right)^k \tag{27}$$

Define a new function variable $p(z)$ as one of the terms in the Laguerre series expansion.

$$p = p(z) = \left(\frac{1-az}{z-a}\right) \tag{28}$$

The numerators of the two Laguerre models can be rewritten into polynomials by replacing the filter terms using this new variable p. Thus the numerator and denominator of the Laguerre models can be written as polynomials of p and z respectively.

$$H_1(z,p) = \left(\frac{\left(b_1^1 + b_2^1 p + \cdots b_{N_1}^1 p^{L_1-1}\right)}{\left(\frac{1}{K}\right)(z-a)} \right) = \frac{N_1(p)}{D_1(z)} \tag{29}$$

$$H_2(z,p) = \left(\frac{\left(b_1^2 + b_2^2 p + \cdots b_{N_1}^2 p^{L_2-1}\right)}{\left(\frac{1}{K}\right)(z-a)} \right) = \frac{N_2(p)}{D_2(z)} \tag{30}$$

If the polynomials, $N_1(p)$ and $N_2(p)$, do not contain common roots, the coefficients of polynomials $H_1'(p)$ and $H_2'(p)$ can be found such that the following polynomial identity is satisfied.

$$N_1(p)H_1'(p) + N_2(p)H_2'(p) = 1 \tag{31}$$

Once the coefficients of the two new polynomials in this identity have been identified through a numerical technique such as pseudo-inverse, two new impulse response models can be defined using the identified polynomials and the denominator of the original Laguerre models.

$$G_1(z,p) = H_1'(p)D_1(z) \tag{32}$$

$$G_2(z,p) = H_2'(p)D_2(z) \tag{33}$$

Finally the common system input, $u(t)$, can be determined by filtering the measured outputs through the inverse filters, $G_1(z,p)$ and $G_2(z,p)$ and then summing the filtered outputs as shown in equation 34.

$$u(t) = G_1(z,p)y_1(t) + G_2(z,p)y_2(t) \tag{34}$$

Proof that the input can be reconstructed using these inverse filters can be shown through proper substitution and cancellation in this equation.

$$u(t) = G_1(z,p)\left(\frac{N_1(p)}{D_1(z)}u(t)\right) + G_2(z,p)\left(\frac{N_2(p)}{D_2(z)}u(t)\right) \tag{35}$$

$$u(t) = H_1'(p)D_1(z)\left(\frac{N_1(p)}{D_1(z)}u(t)\right) + H_2'(p)D_2(z)\left(\frac{N_2(p)}{D_2(z)}u(t)\right) \tag{36}$$

$$u(t) = \left(H_1'(p)N_1(z) + H_2'(p)N_2(z)\right)u(t) \tag{37}$$

The term in parentheses is equal to one given the polynomial identity that was used to calculate $H_1'(p)$ and $H_2'(p)$. The Deconvolution algorithm using the new inverse filters, $G_1(z,p)$ and $G_2(z,p)$ can be represented using two models consisting of a series of filter banks similar to those that were used to represented the Laguerre function series expansion except that each output is first filtered through a common FIR filter corresponding to $D_i(z) = \left(\frac{1}{K}\right)(z-a)$ and uses the coefficients of $H_1'(p)$ and $H_2'(p)$ determined in the polynomial identity as expansion coefficients.

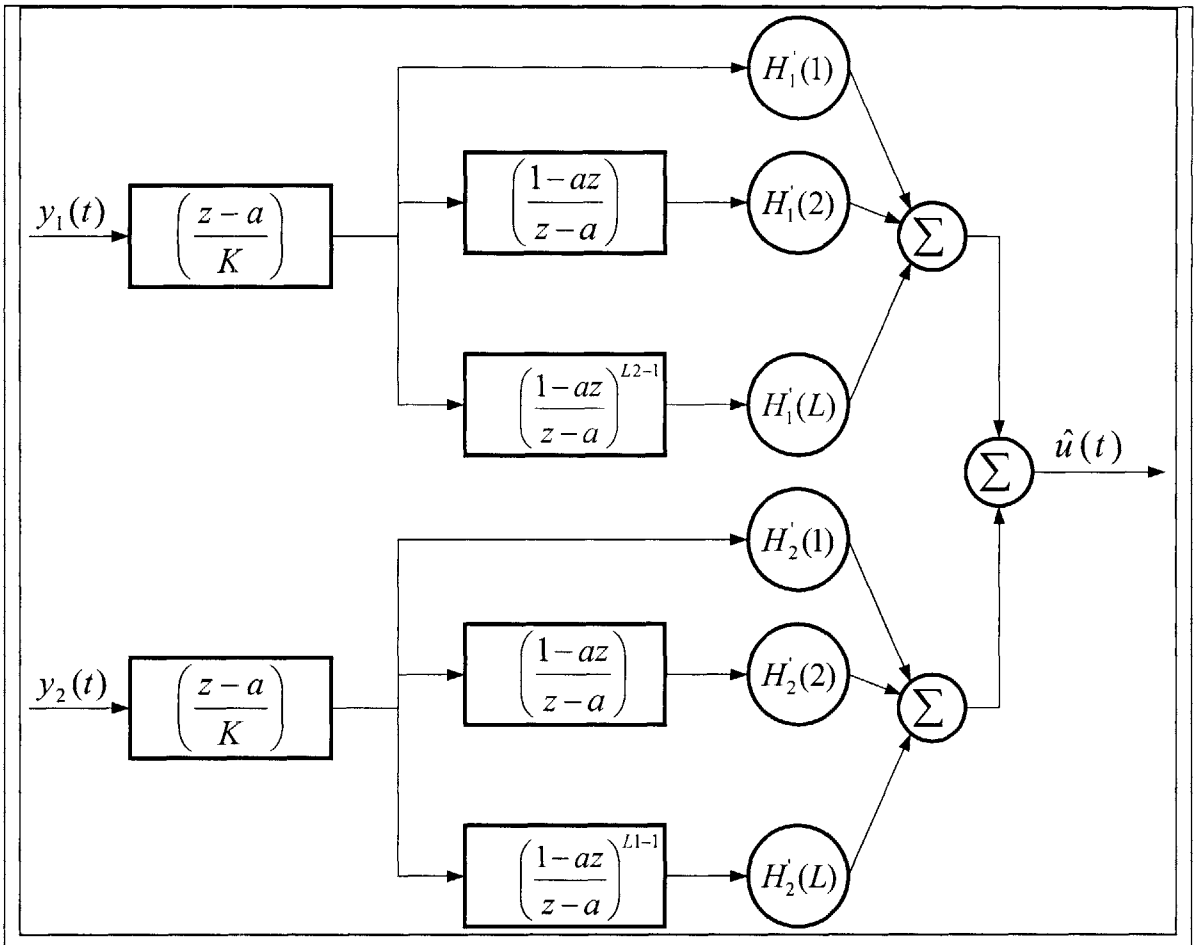

Figure 4: Block diagram of inverse filters for Laguerre model deconvolution

2.5 Implementation of the LaMBSI Algorithm

The procedure for applying the LaMBSI signal-processing algorithm to a time series of measured circulatory signals taken simultaneously from a minimum of two different sensor locations follows a stepwise progression.

1) Select a range of Laguerre poles, a

An estimated range of potential dominant Laguerre poles values, a is selected from the range of all possible pole values for a causal, stable system, $a \in [-1, 1]$.

2) Identify Laguerre model coefficients

A single Laguerre pole value is selected from this range and the coefficients of the Laguerre models are identified by pre-filtering the measured circulatory signal data through the appropriate Laguerre function filter bank and formulating the intermediate filtered data into an over constrained set of linear equations, from which the null space is determined using singular value decomposition.

3) Determine Inverse Filter Coefficients

The coefficients of the inverse deconvolution filters are determined by calculating the coefficients of the polynomials, $H_1^{'}(p)$ and $H_2^{'}(p)$ using the polynomial identity (eqn. 31) and the identified Laguerre model coefficients. A matrix equation of the form $Ax = b$ can be formed by collecting the common terms generated from the polynomial identity, and a pseudoinverse matrix equation is used to determine a minimum solution from the original singular matrix equation.

4) Estimate the common input

The common input to the multi-channel system is estimated from the measured circulatory signals by passing them through their respective inverse deconvolution filters and summing the resulting outputs.

5) Estimate the circulatory signals

Filtering the estimated common input through each of the identified Laguerre models produces estimates of the measured circulatory signals.

6) Compare the estimated and the measured signals

The magnitudes and transport time delay of the estimated circulatory signals, $\hat{y}_i(t)$, which are not preserved using the LaMBSI algorithm are scaled by a common gain to match the magnitudes of the measured circulatory signals, $y_i(t)$. The performances of each of the identified models are evaluated by comparing the estimated circulatory signals with the corresponding measured circulatory signals. The performance measure used for this evaluation is percent data fit (PDF), intuitively a PDF = 100% is an exact recreation of the measured data.

$$PDF = 100 \cdot \left[1 - \frac{\left\| \hat{y}(t) - y(t) \right\|}{\left\| y(t) - mean(y(t)) \right\|} \right] \tag{38}$$

7) Repeat with all potential Laguerre pole values

The first six steps in the procedure are repeated using all the Laguerre pole values in the predetermined range. Therefore, a PDF value is generated for each Laguerre model using every pole value in the range.

8) Identify the optimal Laguerre pole

The Laguerre pole value that produced the highest net performance value, which is determined by summing the PDF values from all the identified Laguerre models corresponding to that pole, is deemed the optimal Laguerre pole. This pole value and the associated models are the outputs of the LaMBSI algorithm.

3. Estimation of Global States using Laguerre Models

3.1 Laguerre Model Representation of Cardiovascular Properties

The Laguerre models identified using LaMBSI can represent the hemodynamic characteristics of the vascular branches with a total of six parameters in each model. Thus, application of the LaMBSI algorithm on the signals derived from two distinct circulatory waveforms generates two vectors, X_1 and X_2 each containing six model parameters.

$$X_1 = \begin{bmatrix} b_1^{(1)} \\ b_2^{(1)} \\ b_3^{(1)} \\ b_4^{(1)} \\ b_5^{(1)} \\ a \end{bmatrix} \text{ and } X_2 = \begin{bmatrix} b_1^{(2)} \\ b_2^{(2)} \\ b_3^{(2)} \\ b_4^{(2)} \\ b_5^{(2)} \\ a \end{bmatrix}$$

An analysis of the foremost arterial wave propagation models [2] show that the hemodynamics of the arterial system are governed by physiologic properties such as the microcirculatory resistance, arterial compliance, and dynamic fluid properties of the blood such as viscosity. Therefore, the two vectors of Laguerre model coefficients produced using the LaMBSI algorithm should exhibit a strong correlation with these physiologic parameters across different cardiovascular states.

The ability to use these model parameters to estimate important physiological variables such as peripheral resistance should be realizable by applying an appropriate statistical model.

3.2 Linear Regression using Laguerre Parameters

A simple linear regression model was used to represent the relationship between the Laguerre model coefficients and total peripheral resistance.

Four different regression models, *f(X)* were tested. Their associated coefficients (β's), were determined so that the LaMBSI parameters would allow estimates of total peripheral resistance using the feature vectors obtained for the individual Laguerre models across different time periods.

$$f(X_1) = \sum_{n=0}^{6} \beta_n X_1(n)$$

$$f(X_2) = \sum_{n=0}^{6} \beta_n X_2(n)$$

$$f(X_1, X_2) = \sum_{n=0}^{6} \beta_n \left(X_1(n) \pm X_2(n)\right)$$

note: In order to identify an intercept the value $X_i(0) = 1$;

The beta coefficients of these regressions were trained using the Laguerre model vectors that had been identified by applying LaMBSI to separate ten second windowed data segments across a time series of data containing two different arterial blood pressure waveforms.

The values of peripheral resistance used to train the regression were obtained by averaging a measured carotid artery pressure waveform, and left ventricular flow over a ten second interval to obtain mean arterial pressure (MAP) and cardiac output (CO) respectively. The ten second data segments used to determine MAP and CO corresponded exactly to those used to identify the Laguerre models parameters with LaMBSI. These two averaged values MAP and CO were used to determine a value for total peripheral resistance (TPR) using a fluid analogy to Ohm's law, with TPR = MAP/CO.

4. Experimental Animal Data

Cardiovascular validation data from a Yorkshire swine (30-34 kg) was studied under an experimental protocol, # 01-055, approved by the MIT Committee on Animal Care shown in Appendix A.

The animal was given intramuscular tiletamine-zolazepam (Telazol), xylazine and atropine prior to endotracheal intubation. Next the swine was maintained in a deep plane of anesthesia with inhaled isoflorane 0.5% - 4%. Positive pressure mechanical ventilation with a respiratory rate of 10-15 breaths/min and a tidal volume of approximately 500 ml was used. Maintenance crystalloid fluids were given once intravenous access was obtained. Two temperature therapy pads were placed on the subjects to maintain a constant core temperature (TPad and TPump,Gaymar Industries, Orchard Park NY).

Physiologic transducers were placed as follows. A temperature probe was inserted in the esophagus (TSD202F, Biopac Systems, Santa Barbara, CA). Needle electrodes (EL452, Biopac Systems) were placed for measuring the electrocardiogram (ECG100C, Biopac Systems) in two standard limb leads. 7.5 French sheath introducers (Arrow International, Reading, PA) were placed in the bilateral femoral arteries under direct visualization after performing cut-downs. Central aortic pressure was measured with a micromanometer-tipped catheter (SPC 350, Millar Instruments, Houston, TX) fed retrograde to the thoracic aorta from the femoral artery. The second introducer was attached to stiff fluid-filled tubing (Arrow International) and an external pressure transducer (TSD104A, Biopac Systems) for measured "*iliac branch*" ABP.

The chest was opened with a midline sternotomy. An ultrasonic flow probe was placed around the aortic root for measuring gold standard Cardiac Output (T206 with A-series probes, Transonic Systems, Ithaca, NY). Acoustic coupling was ensured using bubble-free acoustic gel

and filling the mediastinum with saline to ensure the probe/aortic assembly remained submerged. Finally, following cut-downs in two additional locations, an 18- or 20- gauge angiocatheter was placed in the carotid artery for "*carotid branch*" ABP and a 23- or 25- gauge angiocatheter was placed as distal as possible to the brachial artery in the upper limb for *"radial branch* " ABP. Both were attached to an external pressure transducer by way of a short length of rigid tubing. The analog output of each transduction system was interfaced to a personal computer running Windows 2000 via an A/D system. The data were recorded at a sampling rate of 500 Hz and 16-bit resolution.

A subset of the following interventions was then performed, to vary CO and other hemodynamic parameters, over the course of approximately 75 minutes. The interventions consisted of infusions of hetastarch, crystalloid fluid, phenylephrine, dobutamine, isoproterenol, esmolol, nitroglycerine, and lastly, progressive hemorrhage. Using an infusion pump, infusion rates of these drugs were altered. An observational period typically < 15 minutes took place after each rate change, until either an apparent steady-state was achieved, or an extreme hemodynamic state deemed physiologically unsustainable for the subject was reached. Measurements were made with several infusion rates followed by brief < 15 minute recovery periods to recover baseline conditions between subsequent interventions.

Prior to applying the LaMBSI algorithm to the collected circulatory pressure and flow data it was digitally filtered using an FIR low-pass filter with a 30 Hz cutoff frequency and down sampled to a 100 Hz sampling rate.

Trends in the global cardiovascular parameters identified from a data segment representing nearly an hour of the measured pig data are shown in figure 5. By performing in

real-time the LaMBSI algorithm can adjust to changes in the physiological state and capture the important features of the hemodynamic behavior.

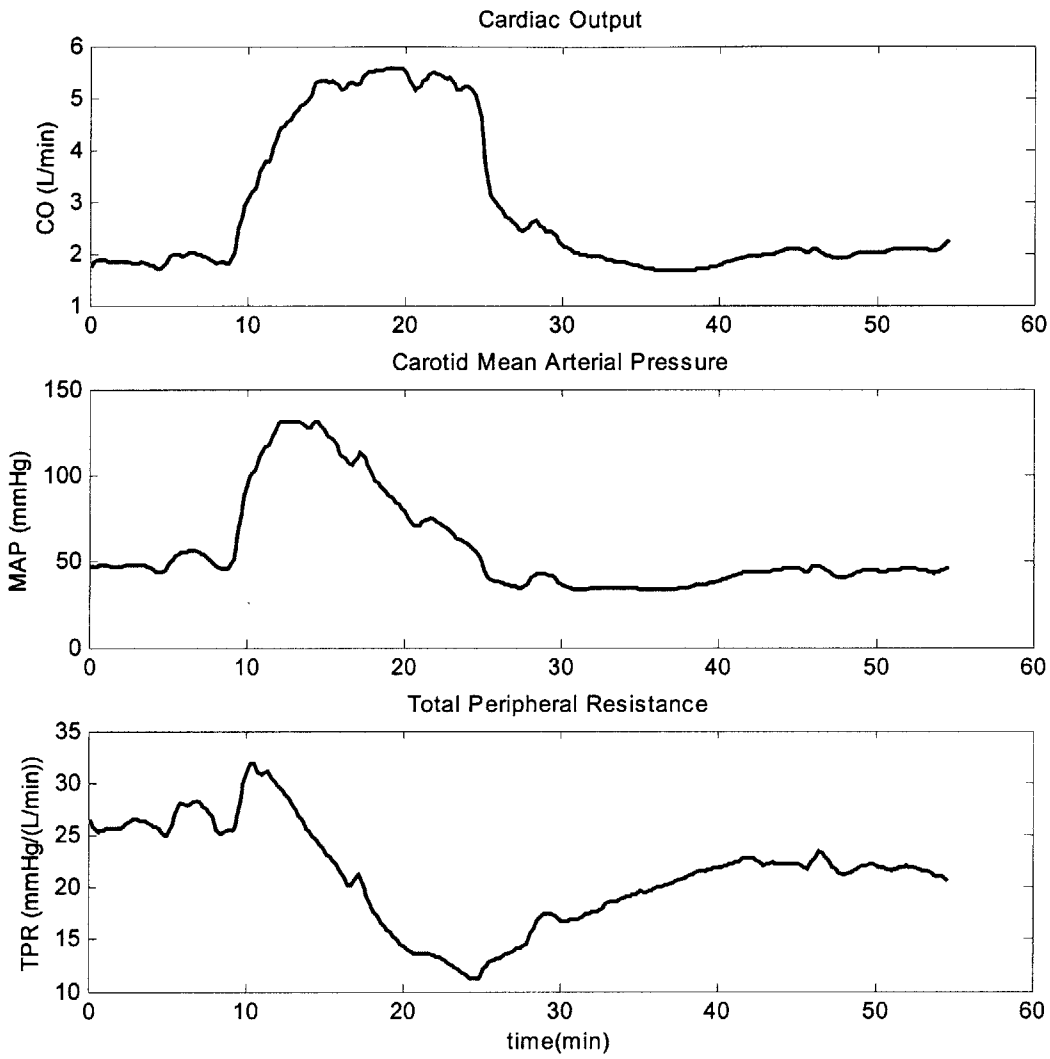

Figure 5: Global cardiovascular trends in the measured swine data

5. Laguerre Model Advantages in Hemodynamic Systems

A powerful advantage of using Laguerre models in the blind system identification algorithm is that they can represent the slow decaying dynamic impulse response of the cardiovascular system with only a small number of expansion coefficients. In addition to reducing the persistence of excitation requirements for the system identification problem, the information content of each of the coefficients within the identified feature vector is greater and they each become stronger predictors of any cardiovascular parameters of interest. In order to evaluate the performance advantages of using Laguerre models in the context of the cardiovascular system, the Laguerre basis expansion can be incorporated into the familiar framework of Least Squares Estimation to identify the expansion coefficients [8].

$$\hat{y}(t \mid \theta) = \varphi^T(t)\theta \tag{43}$$

$$\varphi(t) = \begin{bmatrix} x_0(t) & x_1(t) & \cdots & x_k(t) \end{bmatrix}^T ; \theta = \begin{bmatrix} b_1 & b_2 & \cdots & b_k \end{bmatrix}^T \tag{44}$$

$$\hat{\theta}_N = \left(\sum_{t=1}^{N} \varphi(t)\varphi^T(t) \right)^{-1} \left(\sum_{t=1}^{N} y(t)\varphi(t) \right) \tag{45}$$

5.1 System Identification Performance

Least squares system identification was implemented to identify the hemodynamics of the cardiovascular system using the experimental data derived from the swine model, the system input was the measured cardiac output and the output was the arterial blood pressure waveforms measured in the swine radial artery. The identification was implemented using the batch processing form of the least-squares estimation algorithm. Percentage data fit, PDF and mean

square error, V(θ) performance measures were used to assess the identified FIR models. Least squares estimation was performed on the pig data using both a standard delay operator function model (eqn. 46) and using the Laguerre function model (eqn. 47).

$$\hat{H}(z) = \sum_{k=0}^{L-1} b_k z^{-k} \tag{46}$$

$$\hat{H}(z) = \sum_{k=1}^{L} b_k \frac{K}{(z-a)} \left(\frac{1-az}{z-a} \right)^{k-1} \tag{47}$$

An iterative method was used to identify the minimum number of expansion coefficients required to achieve a PDF of at least 85%. The cardiovascular dynamics were accurately identified and the 85% PDF threshold was reached using a Laguerre function model with 10 expansion coefficients and having a Laguerre pole value of 0.94 (Figure 6). The standard delay operator function model was unable to achieve this PDF value for the experimental data because the regression data matrix became singular to within working precision in the least squares identification algorithm when attempting to identify more than 71 coefficients. Using 71 coefficients the identified standard delay operator model was able to achieve a PDF = 70.3% (Figure 7). The Laguerre model was able to achieve a PDF = 70% using 6 identified expansion coefficients in the least squares algorithm.

The number of coefficients needed to represent the complex cardiovascular dynamics using a standard delay function model is reduced by 91.6% when a Laguerre function model is used instead. In fact, the standard delay operator function models are limited by their high coefficient requirement in the performance that they can actually achieve in modeling the hemodynamics prior to creating a singular matrix condition.

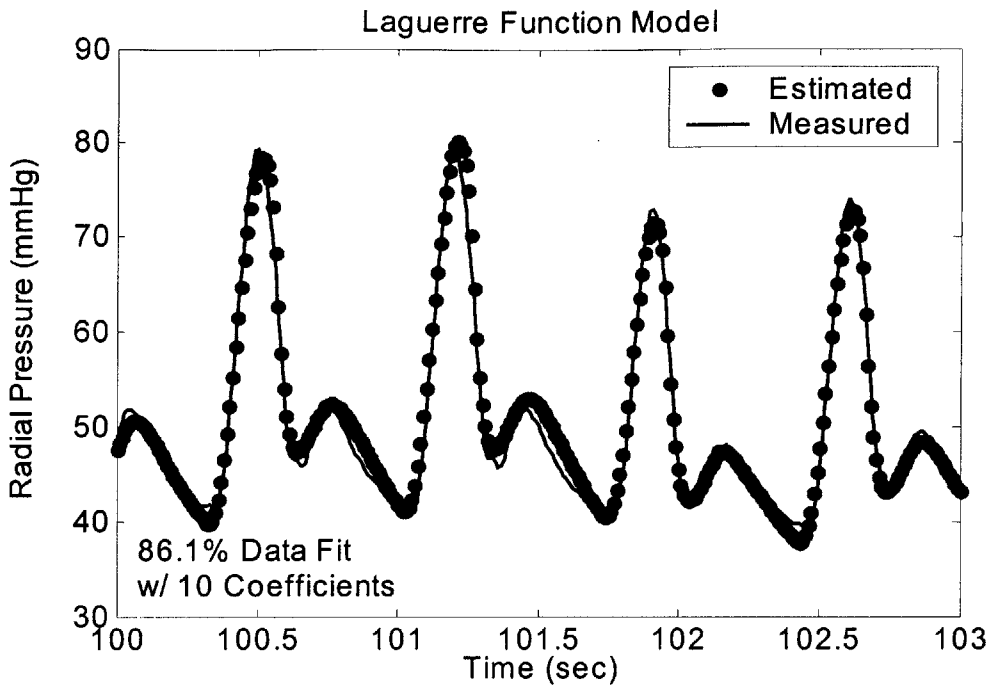

Figure 6: Least squares system ID of swine hemodynamics using a Laguerre model

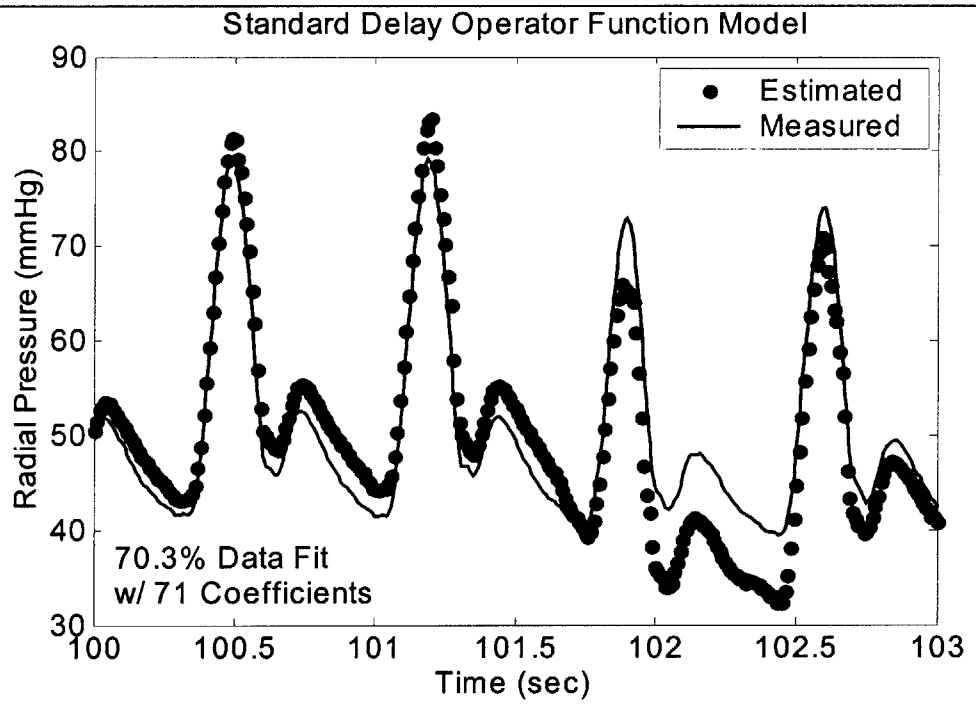

Figure 7: Least squares system ID of swine hemodynamics using a standard FIR model

The number of Laguerre expansion coefficients that will be required by the models identified using the LaMBSI algorithm to model the distinct channel hemodynamics will be even less than that required using the standard least squares system identification algorithm due to the cancellation of a slow decaying dynamic pole because the channels in cardiovascular system are not coprime.

5.2 Effect of the Laguerre Pole on Performance

The estimated Laguerre pole value should reflect an *a priori* knowledge of the slow decaying dynamics of the identified system. In the absence of knowledge about the dominant pole value, for example in a time varying system, an iterative scheme can be implemented to identify the Laguerre pole value that will produce the optimal estimator for the system based on using a predetermined performance measure for model comparison. The identification of the optimal Laguerre pole is possible because the rate of convergence for the Laguerre series expansion to the actual impulse response of the system increases as the Laguerre pole approaches the true value of the actual slow decaying system pole. Therefore, using a fixed number of Laguerre expansion coefficients the optimal Laguerre pole is identified as the pole value that produces a model having the smallest mean squared error value or PDF value closest to 100%. The effect on the mean squared error performance when implementing different values for the Laguerre pole into the least squares system identification algorithm is shown in figure 8. A minimum mean squared error value for the radial artery pressure data was found when a model used a Laguerre pole value, $a = 0.94$.

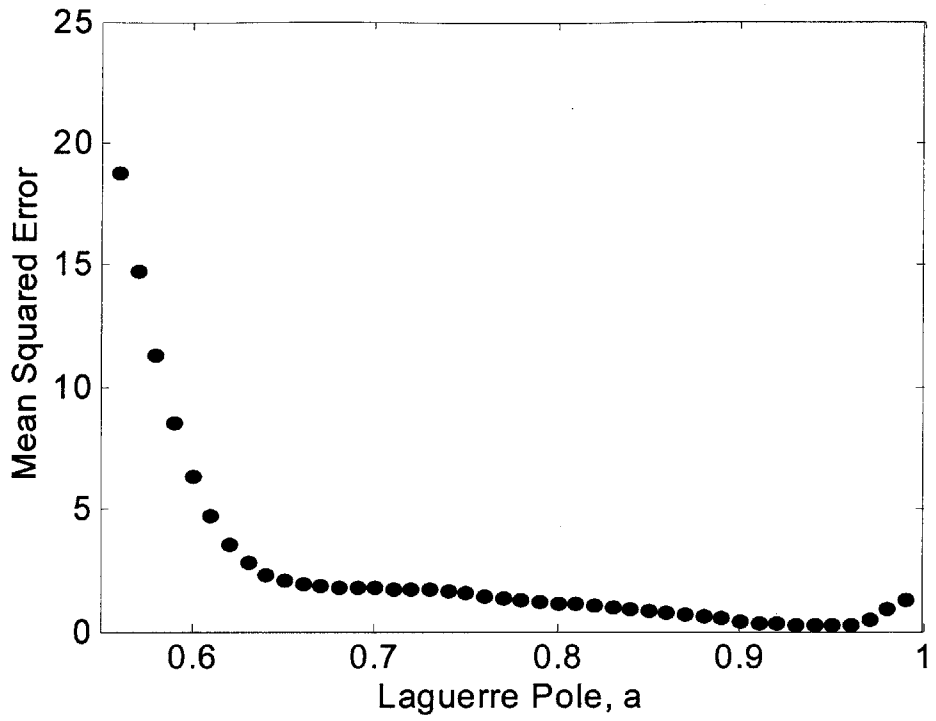

Figure 8: Effect of Laguerre basis pole estimate on Laguerre model performance

6. Blind Identification of Cardiovascular Dynamics

The LaMBSI algorithm was implemented on the experimentally derived cardiovascular data using two of the three measured pressure signals, the measured radial artery blood pressure and the measured iliac artery blood pressure. Individual Laguerre models and their associated parameters were identified from the two pressure waveform signals using isolated ten second data segments taken from the measured time series. The entire data set depicted in figure 5 was divided into non-overlapping ten second data segments and processed using the LaMBSI algorithm. In total, 654 individual Laguerre models were identified using the experimental data

set, 327 corresponding to the measured radial pressures and 327 models corresponding to the measured iliac pressures. These models represent the processing of 654,000 distinct data points.

6.1 Accurate System Identification

The LaMBSI algorithm consistently performed well on the experimental data. Estimated pressure waveforms generated by the identified Laguerre models were excellent reproductions of the measured pressure signals. The ability to reproduce the measured data indicates that the identified Laguerre models had captured a majority of the dynamic behavior and were characteristic of the true system.

The identified Laguerre models were able to accurately reproduce the hemodynamic behavior of the circulatory system throughout the various cardiovascular states contained in the measured data. A portion of the results obtained from using the LaMBSI algorithm to reproduce the measured pressure signals in three different 10-second data segments are shown in figures 9-11. Unique combinations of the three global cardiovascular parameters CO, MAP, and TPR are present in the distinctive waveform features of the three data segments. The reproduced data segments shown in these figures can be mapped to the entire data set depicted in figure 5. The pressure waveforms of Figure 9 were taken at 1.5 minutes, the pressure waveforms of figure 10 were taken at 11.67 minutes, and the pressure waveforms in figure 11 were taken at 21.67 minutes. The performance measure, percentage data fit, was evaluated for all six of the reproduced pressure values shown in the figures above. For the estimates shown in figure 9 the radial channel PDF was 98.8% and the iliac channel PDF was 92.6%. For the estimates depicted in figure 10 the radial channel PDF was 89.1% and the iliac channel PDF was 97.6%. The reproduced pressure data displayed in figure 11 had a radial channel PDF of 97.8% and an iliac channel PDF of 93.8%.

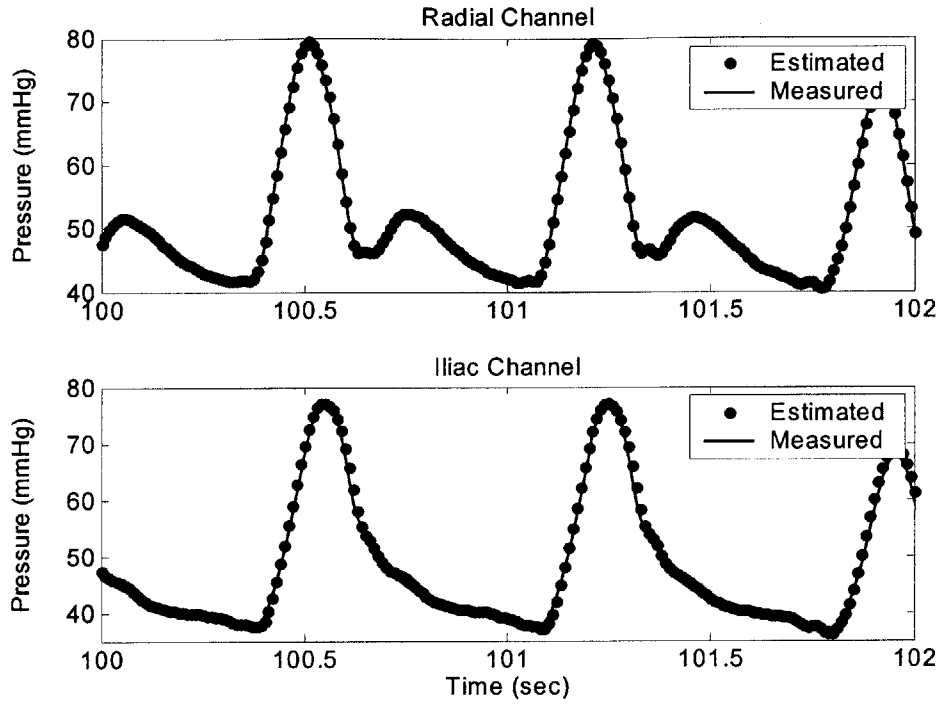

Figure 9: Precise reproduction of normal swine arterial pressure waveforms via LaMBSI

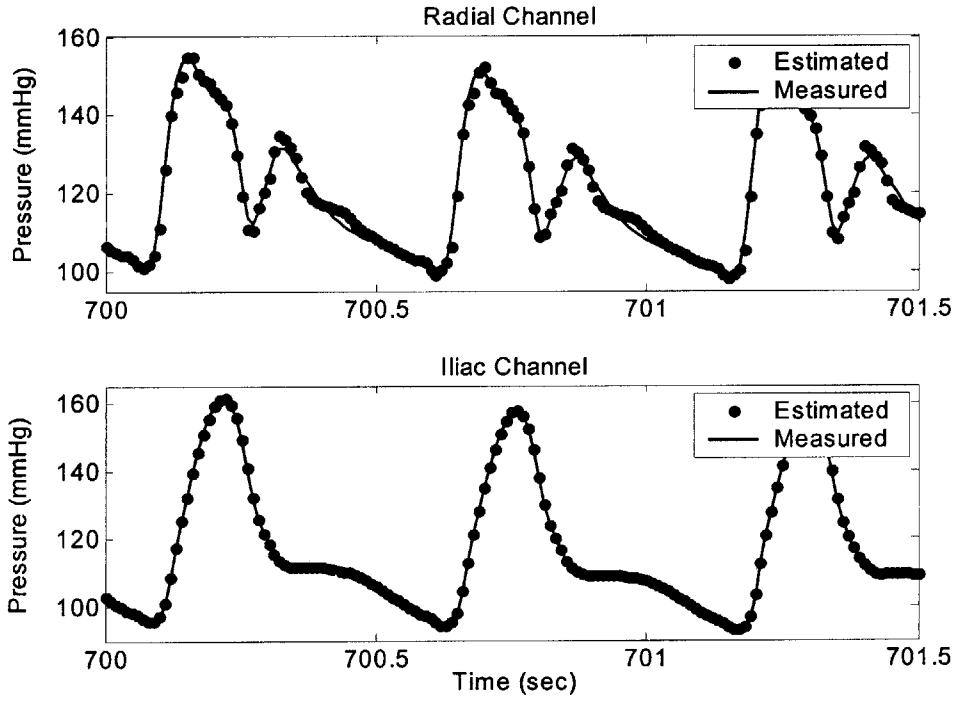

Figure 10: Precise reproduction of elevated swine arterial pressure waveforms via LaMBSI

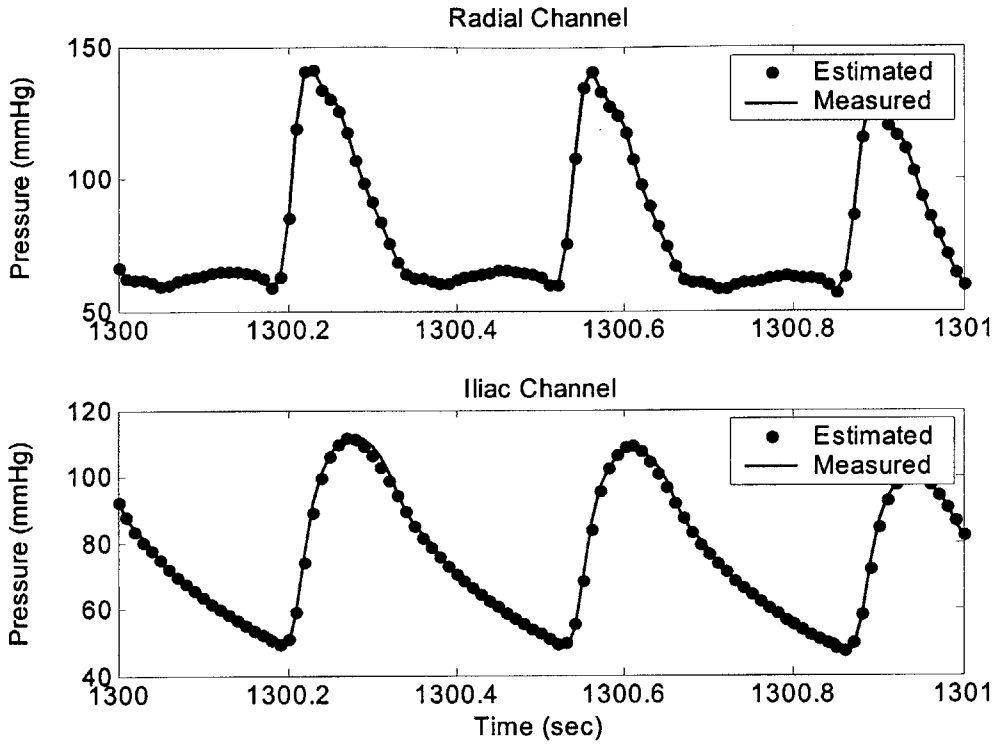

Figure 11: Precise reproduction of swine arterial pressure waveforms having a sub-basal TPR via LaMBSI

Similar PDF results were found throughout the data set. From the 327 pairs of Laguerre models identified using the entire measured data set, the LaMBSI algorithm was able to identify 298 model sets where both the reproduced radial and corresponding iliac waveforms had PDF's > 80%. This translates to a 91.1% success rate. A more detailed examination revealed that 12 of those poor fitting models had pressure data containing catheter-clearing episodes, where the fluid-filled catheters used to measure pressure were flushed to remove blood clots. If the Laguerre model sets corresponding to these data segments are removed the success rate for good models is nearly 95%.

6.2 Local Cardiovascular Characterization

Local cardiovascular characteristics represented by the distinct system dynamics of the specific arterial branch are captured by the model coefficients identified using the LaMBSI algorithm. Sample coefficient values identified using 100 seconds of radial and iliac pressure data are plotted in figure 9. The models were identified using this large data segment to exploit the asymptotic convergence properties of the system identification procedure and produce a minimum variance in the estimated coefficients. The differences in values between the radial and iliac model Laguerre coefficients identified for each channel represent the distinct local dynamic behavior that is contained in the circulatory signals measured at each site.

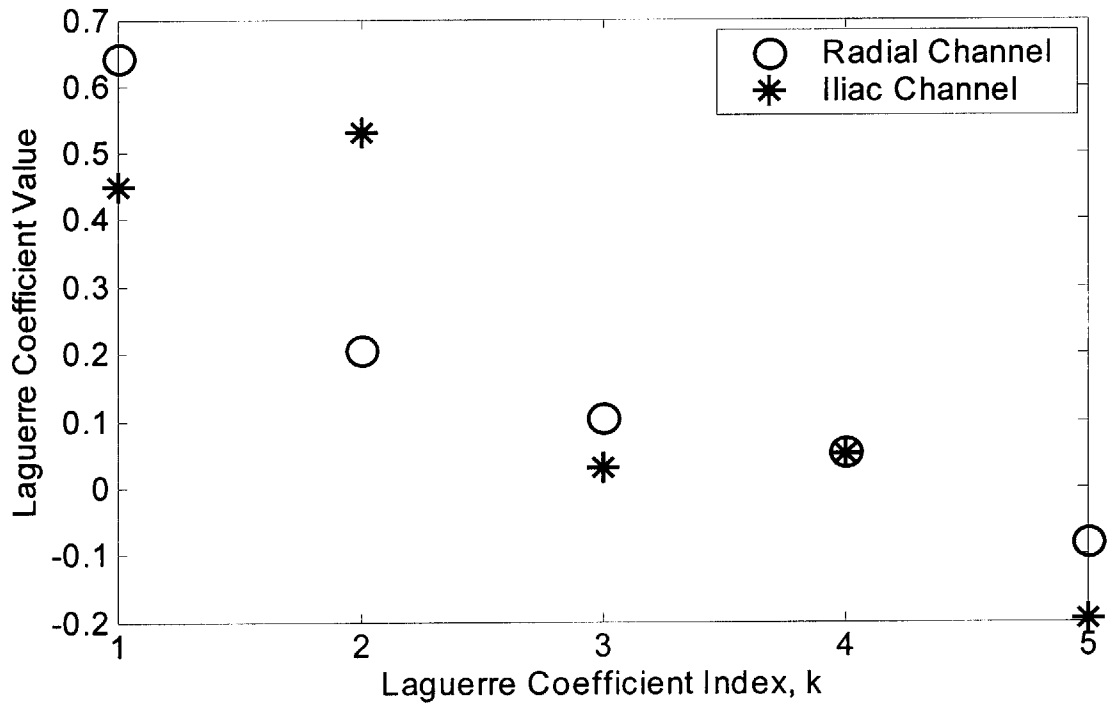

Figure 12: Local circulatory behavior indicated by differences in the Laguerre coefficients identified with LaMBSI from radial and iliac ABP

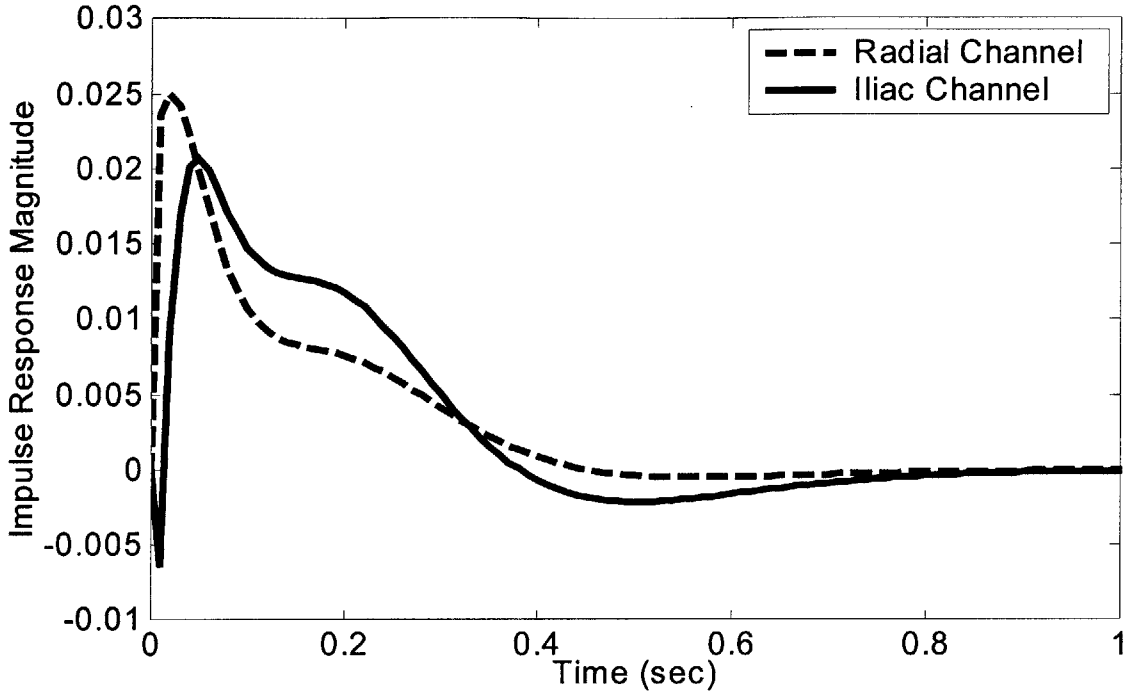

Figure 13: Local circulatory behavior indicated by differences in the impulse response functions of the models identified with LaMBSI from radial and iliac ABP

The two impulse responses that correspond to the models containing the coefficients shown in figure 9 are illustrated in figure 10. The differences in the impulse responses of the two identified Laguerre models reveal the differences in the local cardiovascular dynamics that generated the two measured pressure waveforms. Values taken from either the coefficients directly or from features of the impulse responses may potentially be used to identify specific local cardiovascular phenomenon of interest. The correlation between these features and clinically significant phenomenon will be investigated in the future

6.3 Global Cardiovascular Characterization

Information describing systemic cardiovascular behavior is also contained in the Laguerre model coefficients; however the correlation between global phenomenon and the Laguerre MBSI parameters can be easily recognized in the optimal Laguerre pole value, *a*. Results showing the optimal Laguerre pole values identified using the non-overlapping 10 second data windows across the measured pig pressure data are shown in Figure 5. The changing values of the identified optimal Laguerre pole correspond inversely with the changes in the systemic variable, cardiac output as shown in figure 14.

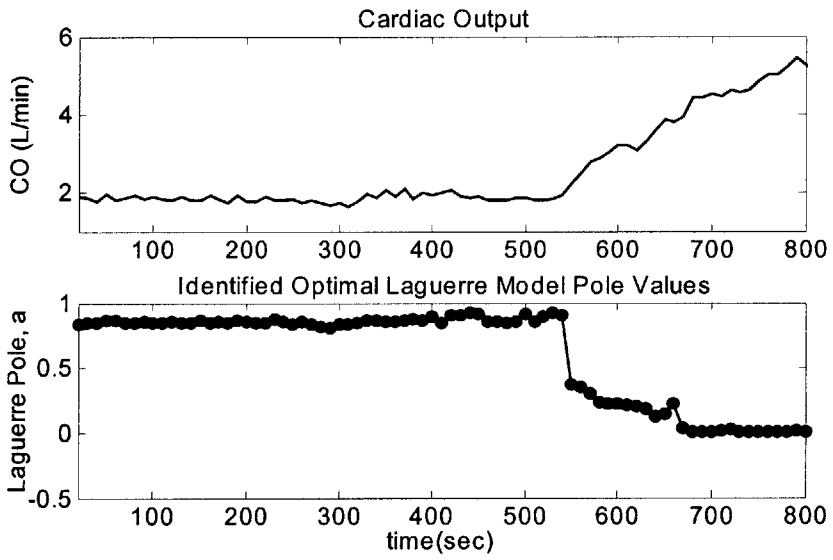

Figure 14: Inverse correlation between the optimal Laguerre basis expansion pole values identified with LaMBSI and cardiac output

Values taken from the identified coefficients and the optimal Laguerre pole should allow the estimation of specific global cardiovascular phenomenon of interest. The correlation between these features and clinically significant phenomenon will be investigated later in this thesis.

7. Estimation of Cardiac Output

7.1 Regression Analysis

The systemic cardiovascular parameters derived from the experimentally measured swine data over a 54-minute period were shown in figure 5. As evidenced by these global parameters CO, MAP, and TPR, the cardiovascular state of the pig was changing throughout the duration of the measurement period.

For all non-overlapping 10-second data segments in the record, LaMBSI was used to identify the coefficients of the Laguerre models using radial and iliac arterial pressure waveform measurements. A total of 327 optimal Laguerre model pairs (radial & iliac) were derived from the data. The identified optimal Laguerre models were each evaluated using the performance measure, percent data fit (PDF).

Laguerre model pairs in which the PDF performance metric was less than 85% for either of the models representing the identified branches (radial or iliac) were removed from the training data set, the data segments for these poor fitting models generally contained some anomalous features, including catheter-clearing episodes where the fluid-filled catheters used to measure pressure were flushed to remove clots. In total, 279 pairs of Laguerre model coefficients were used in the training data set.

The TPR regression models were evaluated using the performance measure mean squared error. The TPR estimator that produced the minimum mean squared error when applied to the data was the linear regression model trained using the difference in Laguerre model coefficient values as the prediction data set (eq. 48-50).

$$TPR(t) = \hat{\beta}^T X(t) \tag{48}$$

$$X(t) = \begin{bmatrix} 1 \\ \left(b_1^{(1)}(t) - b_1^{(2)}(t)\right) \\ \left(b_2^{(1)}(t) - b_2^{(2)}(t)\right) \\ \left(b_3^{(1)}(t) - b_3^{(2)}(t)\right) \\ \left(b_4^{(1)}(t) - b_4^{(2)}(t)\right) \\ \left(b_5^{(1)}(t) - b_5^{(2)}(t)\right) \\ a \end{bmatrix} \tag{49}$$

$$\hat{\beta} = \begin{bmatrix} \beta_0 & \beta_1 & \beta_2 & \beta_3 & \beta_4 & \beta_5 & \beta_6 \end{bmatrix}^T \tag{50}$$

All the Laguerre model prediction data was scaled prior to training and evaluating the linear regression models. Each time series of coefficients having the same coefficient index were scaled by separately multiplying them by the inverse of the standard deviation derived from that time series of coefficients. Thus for the predictor data set 6 different scaling factors were multiplied to the 6 distinct Laguerre model predictor elements.

The outcome data (TPR) used in the training and validation of the linear regression models was also scaled by the inverse of the standard deviation derived from the time series of TPR values.

The time series of Laguerre model parameters and the corresponding TPR values representing a ten second window of measured ABP waveforms were divided into a training data set, used to determine the beta coefficients, $\{\beta_n\}_{n=0,1,2,3,4,5,6}$ of the linear regression, and a validation data set used to evaluate the performance of the linear regression model. To ensure that LaMBSI and TPR data from the different cardiovascular states were well represented in both the training and validation data sets, the data time series was first divided into 3 non-overlapping

parts corresponding to the time intervals, 0-18 minutes, 18-36 minutes, and 36-54 minutes, as shown in figure 15. Each of the three parts contained 93 good sets (PDF's > 85%) of Laguerre model parameters and their corresponding TPR values.

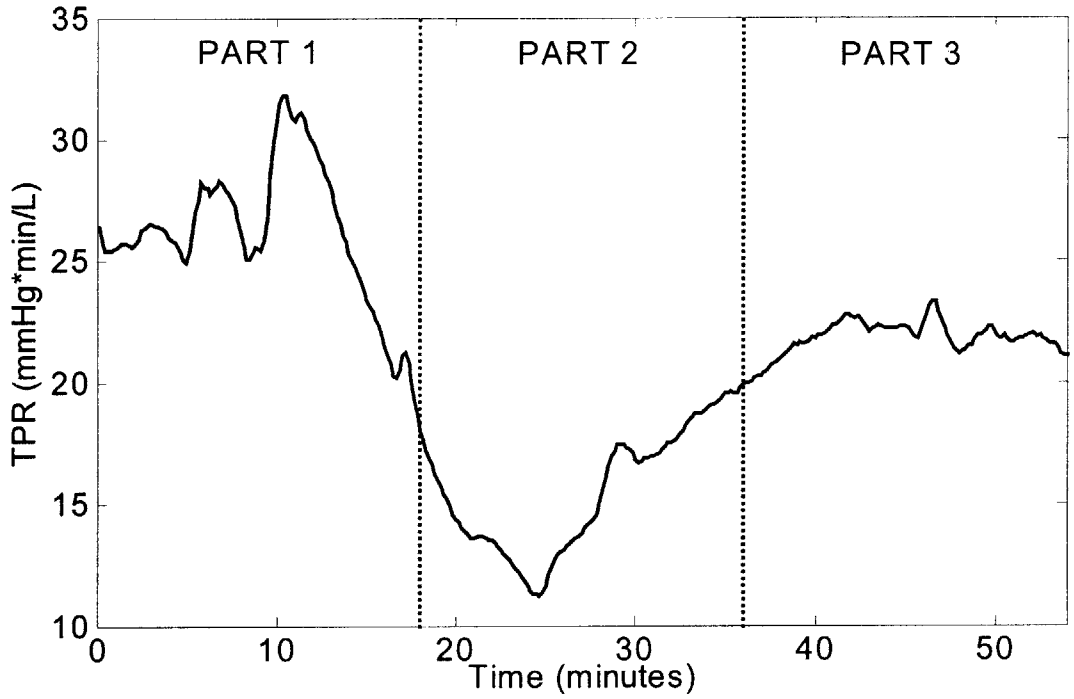

Figure 15: Data parts used for random selection of training and validation data for the regression model

From within each of the three parts in the time series, 1/3 or 31 different sets of Laguerre model parameters were randomly chosen using a uniform distribution of random numbers without replacement to create a validation data set, and the remaining 2/3, or 62 Laguerre model parameters and their TPR values from within that part of the time series were used to form a training data set. In this way, a training data set was randomly generated that contained 186 sets of Laguerre model parameters and the associated TPR values, and a validation data set was generated that contained 93 different sets of Laguerre model parameters and their associated

TPR values. The statistics of the linear regression model generated form the training data set of Laguerre model parameters and TPR values are shown in Table 1.

Regression Coefficient	Mean Value	Standard Error	Lower 95% Confidence Limit	Upper 95% Confidence Limit
β_0	5.15	0.52	4.11	6.19
β_1	0.96	0.22	0.52	1.40
β_2	2.68	0.44	1.80	3.56
β_3	5.47	0.67	4.13	6.81
β_4	4.73	0.45	3.83	5.63
β_5	1.62	0.15	1.32	1.92
β_6	-0.65	0.12	-0.89	-0.41

Table 1: Linear regression model statistics using a training set of Laguerre model parameters as predictors for Total Peripheral Resistance

7.2 Estimation Results

Following determination of the coefficients of the linear regression using the randomly generated training data set, the linear regression model was used to estimate the scaled TPR values based on the previously unseen scaled Laguerre model parameters in the validation data set. The performance of the regression model was measured by evaluating the mean-squared error (MSE) between the estimated and actual scaled TPR values.

$$MSE = \frac{1}{93}\sum_{n=1}^{93}\left(\hat{y}(n) - y(n)\right)^2 \tag{51}$$

Additionally, the performance of the linear regression model was evaluated by determining the correlation coefficient, or r-squared value between the estimated and actual scaled TPR values.

Both of the performance results of the linear regression model on the validation data set are shown in table 2.

Mean Squared Error (MSE)	MSE % of Minimum scaled TPR value	MSE % of Maximum scaled TPR value	TPR r-squared value
0.398	17.2%	6.1%	0.613

Table 2. Performance of the total peripheral resistance linear regression model on the validation data set using Laguerre model coefficients as predictors

The total peripheral resistance values estimated from the linear regression model can be used to provide an estimate of cardiac output given the peripheral ABP measurements. Following a fluid analogy to Ohm's Law cardiac output can be estimated by deriving a mean arterial pressure (MAP) from ten second segments of the measured ABP waveforms and then dividing this value by the TPR values estimated from our regression as described by equation 52.

$$est.CO = \left(\frac{peripheral\ MAP}{est.TPR} \right) \tag{52}$$

Therefore, the cardiac output in the swine model can be estimated from the linear regression model using the LaMBSI parameters identified from the two peripheral arterial blood pressure waveforms. The results for estimating cardiac output are presented in Figure 16 by plotting the relationship between the measured cardiac output and estimated cardiac output.

The points in the plot in Figure 16 should fall along the dashed line having a zero intercept and a unity slope. The actual collection of data points does not lie precisely on this line but their distribution does reveal that the feature vectors identified via LaMBSI and given a peripheral arterial blood pressure measurement have a strong predictive value for estimating cardiac output in the experimental swine model.

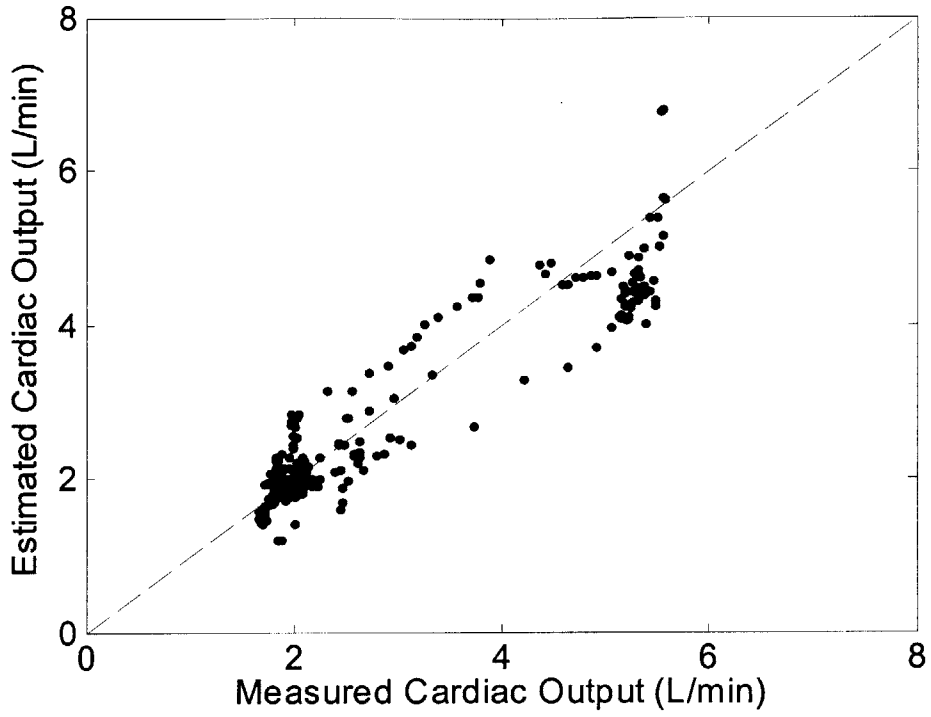

Figure 16: Comparison of estimated cardiac output to measured cardiac output: estimated CO based on a linear regression model using Laguerre model parameters and ABP

7.3 Principal Component Analysis

Based on the results of the linear regression model presented above the difference in the Laguerre model coefficients and the estimated optimal Laguerre pole can be used as strong predictors for estimating total peripheral resistance and cardiac output. In order to develop a better understanding of the physiological variability described by the difference in Laguerre coefficients a principal component analysis (PCA) was performed to reveal the major axes corresponding to this variability and the amount of variability in the direction of these axes.

The vector of inputs used in the PCA analysis corresponded to the data time series of LaMBSI parameters used in the linear regression (eqn. 53).

$$X(t) = \begin{bmatrix} \left(b_1^{(1)}(t) - b_1^{(2)}(t)\right) \\ \left(b_2^{(1)}(t) - b_2^{(2)}(t)\right) \\ \left(b_3^{(1)}(t) - b_3^{(2)}(t)\right) \\ \left(b_4^{(1)}(t) - b_4^{(2)}(t)\right) \\ \left(b_5^{(1)}(t) - b_5^{(2)}(t)\right) \\ a \end{bmatrix} \tag{53}$$

The results of applying PCA on this set of parameters are shown in Table 3 and are depicted graphically in Figure 17. It is very evident that the majority of the variance in this data lies along two principal component directions. The interpretation of this result in the context of the circulatory system is not as evident, but may be very useful for future regression models. The parameters identified in the Laguerre models should provide a characterization of several physiologic features that are related to the dynamics of the cardiovascular system such as total peripheral resistance, arterial compliance, and dynamic fluid properties. The principal components of the Laguerre model parameters may be more closely related to the fluctuations of specific individual physiologic properties that are changing independently and not the result of the superposition of the variation of the many different changing physiologic parameters described by the untransformed Laguerre parameters. Thus, the first principal component alone may represent the variation in the total peripheral resistance in the entire Laguerre parameter set because its variation might be more directly related to the changes that occur only because of the fluctuations in this physiological variable. To continue with this treatment the second component may directly relate to the changes in the arterial compliance of the blood vessels. Thus these two phenomenon, fluctuations in total peripheral resistance and changes in arterial compliance should not be expected to always vary in the same manner and the principal components may depict the individual contributions from each of the two physiologic variables to the Laguerre coefficients. This type of analysis may also help predict specific local phenomenon in the model data,

allowing us to separate the dominating effects of the systemic variables from the more subtle variation caused by local phenomenon.

Principle Component	Variance σ_{ii}	Percent of Total Variance
Component 1	4.4297	73.83
Component 2	1.1665	19.44
Component 3	0.2254	3.76
Component 4	0.1337	2.22
Component 5	0.0426	0.71
Component 6	0.0022	0.04

Table 3: Results from principal component analysis for the Laguerre model parameters

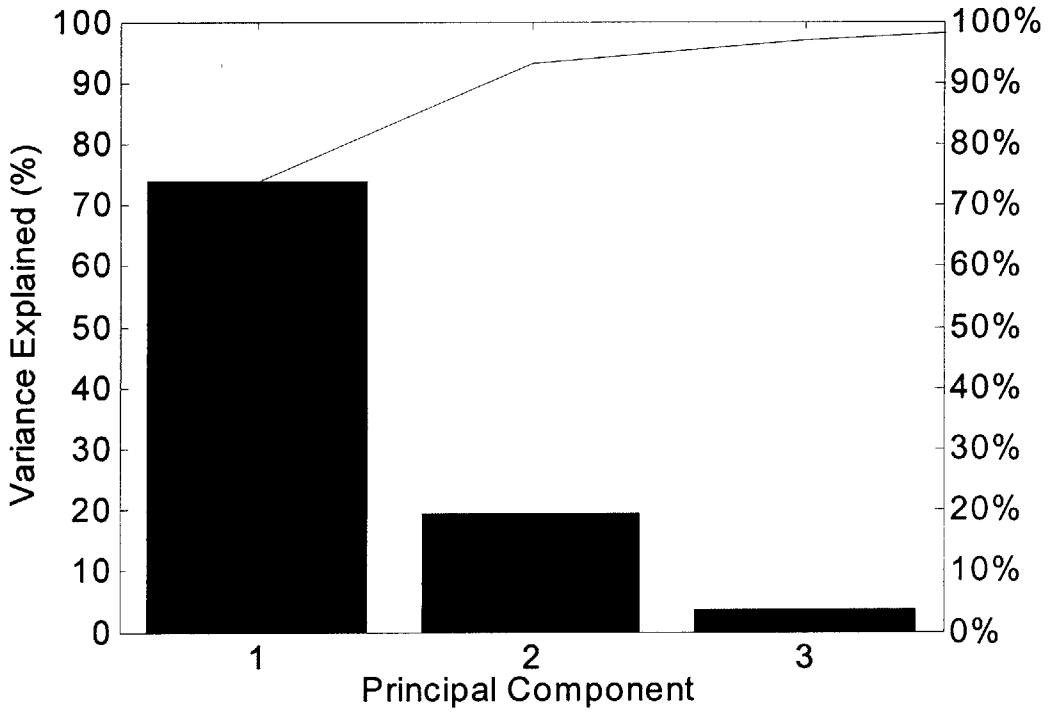

Figure 17: Principal component analysis of the Laguerre model parameters

Chapter 8 – Conclusion

8.1 Summary of Results

A new cardiovascular system identification algorithm, Laguerre Model Blind System ID, has been developed to uniquely characterize both the systemic and local vascular hemodynamics in real-time using peripheral circulatory signals.

A multi-channel blind system identification algorithm has been reformulated to implement a Laguerre basis series expansion. The new Laguerre expansion model provides a compact representation of the cardiovascular system dynamics using an FIR representation and allows blind system identification under the limitations imposed by the cardiovascular system. By using a finite impulse response model the peripheral sensor requirement has been minimized down to only two distinct waveform signals.

A novel deconvolution algorithm has been developed to estimate the common system input in a multi-channel system given two or more identified Laguerre models and their measured output signals. This new algorithm directly identifies model coefficients for the inverse FIR filters using the Laguerre function models.

An iterative step-wise algorithm has been developed to apply LaMBSI to a time-varying system, e.g. the cardiovascular system, not only identifying the coefficients of the Laguerre models, but also estimating the optimal Laguerre pole to use in the Laguerre basis expansion.

This new algorithm overcomes the difficulties associated with applying previously established algorithms in the context of the cardiovascular system and may serve as a platform for applying blind system identification to any dynamic system providing a compact finite series model representation for systems with a slow decaying impulse response or fixed low complexity input.

This new LaMBSI algorithm has been applied to experimental cardiovascular data derived from a swine model and shown to consistently identify the dynamics of the cardiovascular system across changing physiologic states.

LaMBSI has been shown as a means of quantifying both systemic and local circulatory phenomenon from the experimental circulatory data. Therefore, LaMBSI offers a new tool for consistently characterizing cardiovascular parameters without the confounding effects created by the distributed topology of the cardiovascular system.

An initial proof-of-principle has been provided showing that the identified LaMBSI model vectors can be used to estimate a physiologic parameter of interest, namely TPR.

A trained linear regression model using the Laguerre model parameter vectors can be used to estimate values of total peripheral resistance across changing cardiovascular states. Additionally, given a measured arterial blood pressure value these feature vectors can be used to estimate cardiac output.

This straightforward example shows the possible utility of the identified hemodynamic model parameters and using these feature vectors with similar techniques may permit the quantification of other global arterial parameters such as total compliance or identification of local vascular pathology.

The variance contained in the set of Laguerre model parameters has been found to lie in two principal directions, and it has been hypothesized that the variance along the component directions may represent the variance of specific individual physiologic variables contained in the Laguerre parameters.

8.2 Future Research Directions

Future theoretical research directions for the LaMBSI algorithm will include identification of the optimal window size from which to identify the Laguerre models. Based on the time rate of change of the different physiologic parameters of the cardiovascular system a procedure should be developed to find the length of the data segment that will allow identification using the maximum window size, a longer data segment will leverage the asymptotic convergence properties of the system identification problem reducing the variance in the identified coefficients. An improved objective function, other than PDF, should be identified and implemented for estimating the optimal Laguerre pole. This new function should be used to reduce the variance associated with identifying this parameter of the series expansion.

The performance of the LaMBSI parameter linear regression model should be compared with other techniques for estimating cardiac output. Systemic parameter estimation using the PCA projected data should be implemented through a linear regression model and physiologically meaningful explanations of the two principal components should be established.

There are several future research topics that must be addressed prior to the application of this technology in a clinical setting. The performance of the LaMBSI algorithm should be verified using ABP data from at least ten different swine models.

Additionally, because twin arterial blood pressure measurements may not always be feasible in clinical settings future work will include investigation into using LaMBSI with less invasive hydrodynamic signals, these different wearable sensor modalities could include electrical-impedance plethysmography and/or photoplethysmography. Once non-invasive signals can be used to quantify the hemodynamics, characterization of human circulatory parameters should be evaluated.

References

[1] Y. Zhang and Asada H, "Multi-Channel Blind System Identification for Central Hemodynamic Monitoring" *ASME Journal of Dynamic Systems, Measurements, and Control*, accepted for publication.

[2] W. O'Rourke ed., M, McDonald's *Blood Flow in Arteries: Theoretical, Experimental and Clinical Principles*, Oxford University Press, London, 1997.

[3] Y.C. Fung, *Biomechanics: Circulation*, Springer, New York, 1996.

[4] G. Xu, *et al.*, "A Least-squares approach to blind channel identification," *IEEE Transactions on Signal Processing*, 43(12), pp. 2982 – 2993, 1995.

[5] M. I. Gurelli and C. L. Nikias, "EVAM: an eigenvector-based algorithm for multichannel blind deconvolution of input colored signals," *IEEE Transactions on Signal Processing*, 43(1), pp. 134 – 149, 1995

[6] P. Van Den Hof, *et al.*, "System Identification with Generalized Orthonormal Basis Functions," *Automatica*, 31(12), pp. 1821 – 1834, 1995.

[7] L. Ljung, *System Identification*, Prentice Hall, Upper Saddle River, NJ, 1999.

[8] B. Wahlberg, "System Identification Using Laguerre Models", *IEEE Transactions on Automatic Control*, 36(5), pp. 551-562, 1991.

[9] P. Heuberger, P. Van Den Hof, and O. Bosgra, "A Generalized Orthonormal Basis for Linear Dynamical Systems," *IEEE Transactions on Automatic Control*, 40(3), pp. 451-465, 1995.

[10] Wesseling, K.H., et al., "Computation of aortic flow from pressure in humans using a nonlinear, three-element model." J Appl Physiol, 1993. **74**(5): p. 2566-73.

[11] Godje, O., et al., "Reliability of a new algorithm for continuous cardiac output determination by pulse-contour analysis during hemodynamic instability." Crit Care Med, 2002. **30**(1): p. 52-8.

[12] Hamilton, T.T., L.M. Huber, and M.E. Jessen, "PulseCO: a less-invasive method to monitor cardiac output from arterial pressure after cardiac surgery." Ann Thorac Surg, 2002. **74**(4): p. S1408-12.

[13] Wesseling, K.H., et al., "A computer module for the continuous monitoring of cardiac output in the operating theatre and the ICU" Acta Anaesthesiol Belg, 1976. **27 suppl**: p. 327-41.

[14] Fay, J. A., Introduction to Fluid Mechanics, MIT Press, Cambridge, MA, 1994

Appendix A. Animal Experiment Protocol

MASSACHUSETTS INSTITUTE OF TECHNOLOGY
COMMITTEE ON ANIMAL CARE
BLDG. 16-408
CAMBRIDGE, MA 02139
tel. 617 253-9436/fax 617 258-8257
NOTICE OF COMMITTEE REVIEW

Date: November 5, 2001
Proposal #: 01-055
Proposal Title: Multi-channel Blind System Identification for Noninvasive Cardiovascular Monitoring
Principal Investigator: Harry Asada/Andrew Reisner Department: MEC
Funding Agency: Harvard/MIT Center for Integration of Medicine and Innovative Technology (CIMIT)
Grant #: pending

x New Proposal	___ Three-year Renewal	___ Annual Renewal
___ Addendum	___ Teaching Proposal	___ Expedited Review

The above-named proposal was reviewed at the November 1, 2001 meeting of the Committee on Animal Care. This is to inform you of the following:

x Approval*

___ Approval with the provisions listed below.

___ Approval limited to ___ days, pending receipt of the additional information requested below.

___ Approval deferred pending receipt of information requested below.

___ Disapproved for the reasons described below.

The following provisions and/or suggestions have been made by the CAC:

Reasons for disapproval:

*Projects involving the use of biohazardous material (radioisotopes, infectious agents, carcinogens, as examples) require separate approval by the Radiation Protection Office, Industrial Hygiene Office/ Environmental Medical Service, or the Biosafety Office. The Committee on Animal Care approval is contingent on the approval of these separate MIT committees. Animal work should not commence until all approvals have been received by the Principal Investigator.

This institution has an Animal Welfare Assurance on file with the Office for Laboratory Animal Welfare. The Assurance number is A-3125-01.

Action described in this notice applies for 12 months from the date of approval or the time indicated and is based on the assumption that no substantive changes in experimental procedures dealing with animals used will occur during the period unless approval for the revised procedure(s) is obtained from the Committee on Animal Care.

Chair, CAC

Assoc. Dir, Office of Sponsored Programs/Grants Management

Appendix B. LaMBSI Data

a	$b_1[1]$	$b_1[2]$	$b_1[3]$	$b_1[4]$	$b_1[5]$	$b_2[1]$	$b_2[2]$	$b_2[3]$	$b_2[4]$	$b_2[5]$	Radial Fit	Iliac Fit	CO (L/min)	MAP (mmHg)	TPR (MAP/CO)
0.84	0.668	0.164	0.162	0.056	0.008	0.428	0.522	0.064	0.122	-0.148	91.91	98.43	1.78	46.91	26.42
0.85	0.670	0.138	0.098	0.069	-0.072	0.451	0.509	-0.016	0.096	-0.200	92.38	97.36	1.84	47.26	25.75
0.85	0.617	0.243	0.234	0.029	0.033	0.415	0.525	0.177	0.089	-0.127	88.75	98.41	1.87	47.53	25.45
0.87	0.615	0.259	0.092	0.041	-0.098	0.446	0.545	0.043	0.009	-0.196	91.68	98.84	1.88	47.70	25.43
0.87	0.623	0.230	0.063	0.019	-0.124	0.456	0.531	0.006	-0.015	-0.221	88.11	98.27	1.88	47.76	25.45
0.85	0.606	0.267	0.224	0.040	0.037	0.405	0.537	0.183	0.089	-0.119	91.40	99.08	1.87	47.71	25.51
0.85	0.658	0.180	0.169	0.044	-0.026	0.444	0.514	0.082	0.085	-0.168	90.85	98.52	1.86	47.59	25.58
0.86	0.583	0.306	0.207	0.060	0.000	0.400	0.552	0.181	0.078	-0.132	88.11	98.60	1.85	47.53	25.70
0.85	0.646	0.206	0.178	0.046	-0.009	0.435	0.524	0.104	0.087	-0.155	92.63	98.75	1.85	47.49	25.72
0.85	0.666	0.157	0.143	0.054	-0.046	0.447	0.513	0.041	0.092	-0.184	92.21	97.99	1.85	47.44	25.69
0.86	0.640	0.214	0.108	0.051	-0.073	0.448	0.533	0.039	0.049	-0.192	92.55	98.82	1.85	47.34	25.65
0.85	0.599	0.279	0.227	0.052	0.046	0.397	0.541	0.192	0.098	-0.106	92.69	98.87	1.85	47.36	25.59
0.85	0.573	0.313	0.240	0.058	0.066	0.376	0.547	0.225	0.101	-0.083	92.71	97.10	1.85	47.51	25.74
0.87	0.627	0.209	0.060	-0.002	-0.130	0.458	0.525	-0.006	-0.025	-0.239	90.36	98.38	1.84	47.73	25.95
0.85	0.584	0.297	0.240	0.061	0.055	0.373	0.547	0.215	0.112	-0.093	89.72	97.93	1.83	47.88	26.25
0.86	0.663	0.154	0.091	0.048	-0.101	0.452	0.514	-0.011	0.054	-0.212	92.49	97.20	1.82	47.96	26.35
0.85	0.583	0.304	0.232	0.059	0.065	0.365	0.555	0.210	0.115	-0.086	92.15	96.90	1.81	48.05	26.52
0.87	0.617	0.260	0.087	0.040	-0.099	0.426	0.556	0.044	0.017	-0.201	87.04	98.69	1.82	48.23	26.55
0.86	0.548	0.339	0.259	0.050	0.053	0.361	0.547	0.256	0.091	-0.091	91.54	97.02	1.83	48.34	26.49
0.85	0.592	0.285	0.249	0.037	0.059	0.379	0.538	0.220	0.101	-0.100	89.92	97.30	1.83	48.36	26.41
0.85	0.584	0.299	0.245	0.040	0.067	0.374	0.542	0.226	0.101	-0.092	91.70	96.37	1.82	48.09	26.40
0.88	0.540	0.368	0.168	0.029	-0.060	0.397	0.571	0.170	0.000	-0.166	90.16	97.09	1.80	47.57	26.38
0.86	0.640	0.224	0.093	0.070	-0.072	0.422	0.549	0.032	0.072	-0.190	89.44	98.45	1.78	46.69	26.23
0.84	0.667	0.179	0.184	0.020	0.051	0.405	0.531	0.100	0.114	-0.130	91.61	98.08	1.76	45.80	26.00
0.86	0.578	0.327	0.182	0.054	0.026	0.382	0.571	0.168	0.082	-0.123	92.35	99.41	1.74	45.00	25.85
0.84	0.686	0.041	0.017	0.090	-0.088	0.421	0.490	-0.143	0.148	-0.227	93.04	96.55	1.72	44.40	25.80
0.82	0.715	-0.180	0.139	0.007	-0.035	0.406	0.384	-0.174	0.204	-0.226	95.27	93.89	1.72	43.98	25.64
0.81	0.699	-0.188	0.099	0.012	-0.015	0.379	0.402	-0.238	0.236	-0.219	94.92	95.80	1.74	44.09	25.39
0.84	0.688	0.087	0.092	0.005	-0.026	0.425	0.516	-0.056	0.115	-0.217	93.48	98.62	1.80	45.06	25.10
0.84	0.659	0.185	0.211	-0.024	0.062	0.410	0.522	0.128	0.090	-0.136	92.50	97.78	1.88	46.87	24.97
0.85	0.629	0.245	0.191	0.020	0.017	0.402	0.544	0.140	0.088	-0.149	88.87	98.42	1.93	49.07	25.44
0.87	0.502	0.391	0.259	0.065	0.021	0.349	0.555	0.279	0.075	-0.098	89.05	98.16	1.98	51.41	25.97
0.87	0.482	0.411	0.260	0.100	0.020	0.331	0.559	0.289	0.093	-0.080	88.68	99.52	1.97	53.17	27.03
0.86	0.504	0.375	0.291	0.074	0.043	0.336	0.538	0.308	0.104	-0.078	87.49	97.38	1.98	54.43	27.57
0.86	0.502	0.380	0.288	0.096	0.050	0.321	0.538	0.312	0.124	-0.061	87.97	97.83	1.95	54.79	28.22
0.87	0.645	0.217	0.105	-0.016	-0.108	0.433	0.532	0.060	-0.038	-0.196	87.85	97.53	1.97	55.18	28.04
0.88	0.559	0.342	0.195	-0.010	-0.059	0.400	0.552	0.196	-0.026	-0.157	85.39	95.32	1.98	55.53	28.02
0.87	0.636	0.244	0.121	0.000	-0.099	0.424	0.539	0.086	-0.022	-0.181	88.99	98.26	2.03	56.19	27.73
0.9	0.432	0.471	0.259	0.051	-0.040	0.319	0.569	0.292	0.014	-0.094	88.38	93.81	2.03	56.63	27.97
0.92	0.456	0.391	-0.077	-0.233	-0.173	0.369	0.522	-0.038	-0.325	-0.185	74.94	82.97	2.01	56.63	28.14
0.85	0.708	0.021	-0.001	0.066	-0.162	0.424	0.474	-0.121	0.034	-0.217	92.24	92.07	1.99	56.25	28.28
0.91	0.530	-0.513	0.371	-0.228	0.148	0.465	-0.142	-0.064	0.060	-0.030	92.48	87.27	1.97	55.50	28.20

0.98	0.142	0.341	0.504	0.292	0.038	0.091	0.330	0.562	0.297	-0.040	63.55	75.17	1.97	54.80	27.92
0.91	0.547	-0.487	0.346	-0.264	0.136	0.487	-0.111	-0.071	0.003	-0.046	91.12	89.87	1.94	53.85	27.82
0.92	0.086	-0.186	-0.496	-0.412	-0.200	0.091	-0.072	-0.479	-0.469	-0.199	28.36	37.09	1.92	52.71	27.52
0.93	0.665	-0.159	-0.076	-0.166	0.088	0.590	0.131	-0.325	-0.128	0.060	88.53	81.69	1.87	51.13	27.27
0.92	0.451	0.341	-0.080	-0.256	-0.157	0.389	0.506	-0.041	-0.354	-0.220	79.68	88.71	1.84	49.38	26.80
0.92	0.452	0.348	-0.038	-0.248	-0.148	0.395	0.518	-0.006	-0.336	-0.230	84.13	91.05	1.82	47.79	26.24
0.86	0.681	0.118	0.076	0.040	-0.096	0.450	0.504	-0.033	0.052	-0.213	92.49	96.95	1.82	46.63	25.58
0.86	0.684	0.090	0.094	0.004	-0.102	0.462	0.483	-0.035	0.037	-0.233	93.23	95.74	1.84	46.11	25.11
0.85	0.703	0.024	0.122	0.001	-0.078	0.458	0.460	-0.046	0.079	-0.234	94.49	95.19	1.84	46.02	25.07
0.86	0.687	0.026	0.068	-0.027	-0.141	0.463	0.453	-0.094	0.018	-0.271	93.67	92.02	1.82	46.27	25.39
0.92	0.441	0.371	-0.033	-0.240	-0.163	0.380	0.528	-0.001	-0.326	-0.232	85.31	90.69	1.83	46.76	25.59
0.86	0.690	-0.007	0.103	-0.049	-0.145	0.447	0.451	-0.095	0.027	-0.279	93.20	88.09	1.89	48.18	25.54
0.9	0.549	0.252	0.007	-0.211	-0.171	0.420	0.505	-0.021	-0.239	-0.270	82.71	93.16	2.03	51.65	25.45
0.93	0.691	-0.153	0.248	-0.124	0.078	0.591	0.205	-0.063	0.081	-0.121	85.67	91.94	2.25	58.29	25.83
0.91	0.611	-0.382	0.299	-0.243	0.102	0.539	0.012	-0.102	0.052	-0.133	87.60	88.04	2.49	67.65	26.94
0.37	0.228	-0.575	0.653	-0.395	0.105	0.071	-0.074	-0.027	0.102	-0.056	86.44	90.14	2.72	77.86	28.45
0.35	0.259	-0.603	0.609	-0.328	0.083	0.052	0.025	-0.180	0.203	-0.081	91.56	87.82	2.90	86.98	29.89
0.3	0.251	-0.598	0.622	-0.350	0.093	0.044	0.024	-0.156	0.172	-0.067	92.28	85.39	3.04	93.96	30.86
0.24	0.258	-0.586	0.602	-0.364	0.111	0.026	0.080	-0.201	0.177	-0.060	96.62	88.67	3.13	98.56	31.48
0.23	0.255	-0.588	0.613	-0.373	0.113	0.030	0.058	-0.170	0.158	-0.056	96.81	88.83	3.18	101.15	31.79
0.23	0.252	-0.585	0.626	-0.400	0.127	0.040	0.019	-0.107	0.110	-0.042	97.32	88.48	3.25	103.10	31.79
0.22	0.260	-0.588	0.618	-0.393	0.126	0.034	0.036	-0.124	0.119	-0.045	97.35	90.17	3.39	106.05	31.36
0.21	0.274	-0.595	0.602	-0.384	0.129	0.032	0.053	-0.143	0.130	-0.048	97.83	90.58	3.57	110.30	30.92
0.19	0.262	-0.596	0.620	-0.389	0.124	0.037	0.021	-0.102	0.108	-0.043	96.72	89.98	3.72	114.39	30.80
0.13	0.246	-0.585	0.632	-0.407	0.130	0.036	0.005	-0.075	0.083	-0.033	97.64	88.97	3.77	116.77	31.00
0.15	0.243	-0.573	0.635	-0.427	0.142	0.039	-0.010	-0.042	0.056	-0.025	97.59	87.27	3.78	117.58	31.12
0.23	0.266	-0.579	0.620	-0.422	0.147	0.045	0.000	-0.052	0.067	-0.030	97.64	89.00	3.87	119.36	30.84
0.08	0.220	-0.551	0.645	-0.451	0.149	0.047	-0.057	0.026	0.008	-0.011	96.23	79.74	4.04	122.83	30.41
0.96	0.329	0.569	0.235	-0.105	-0.071	0.300	0.574	0.246	-0.101	-0.085	77.94	74.85	4.24	127.38	30.08
0.04	0.223	-0.568	0.649	-0.426	0.133	0.046	-0.057	0.015	0.023	-0.015	97.10	85.45	4.36	129.90	29.83
0.01	0.223	-0.562	0.645	-0.435	0.140	0.026	0.008	-0.067	0.067	-0.023	98.45	85.62	4.41	130.77	29.65
0.01	0.214	-0.544	0.649	-0.460	0.153	0.037	-0.035	0.003	0.013	-0.006	99.01	84.05	4.47	130.65	29.24
0.01	0.219	-0.565	0.651	-0.427	0.133	0.028	-0.004	-0.052	0.061	-0.022	97.22	78.96	4.52	130.77	28.94
0.01	0.226	-0.584	0.649	-0.397	0.115	0.026	0.008	-0.081	0.090	-0.033	96.59	83.36	4.58	130.95	28.58
0.02	0.232	-0.593	0.645	-0.383	0.109	0.028	0.007	-0.087	0.100	-0.038	96.06	84.98	4.63	131.06	28.33
0.03	0.231	-0.592	0.650	-0.390	0.111	0.036	-0.023	-0.046	0.074	-0.032	96.38	83.46	4.70	131.18	27.92
0.01	0.227	-0.583	0.651	-0.404	0.119	0.037	-0.029	-0.030	0.058	-0.026	96.47	81.47	4.78	130.98	27.42
0.01	0.230	-0.580	0.647	-0.412	0.126	0.036	-0.026	-0.032	0.058	-0.025	96.79	81.07	4.85	130.37	26.88
0.01	0.224	-0.568	0.649	-0.428	0.135	0.038	-0.038	-0.007	0.035	-0.017	96.66	78.83	4.89	129.44	26.49
0.01	0.227	-0.570	0.646	-0.428	0.136	0.036	-0.029	-0.018	0.041	-0.018	97.29	81.44	4.92	128.36	26.10
0.01	0.225	-0.566	0.647	-0.432	0.139	0.038	-0.038	-0.002	0.028	-0.014	97.07	79.55	4.95	127.70	25.80
0.01	0.230	-0.564	0.641	-0.440	0.147	0.037	-0.029	-0.014	0.034	-0.015	97.89	81.59	5.07	128.17	25.30
0.01	0.220	-0.558	0.648	-0.440	0.142	0.028	-0.008	-0.040	0.053	-0.021	95.87	75.40	5.19	129.69	24.99
0.01	0.249	-0.586	0.623	-0.404	0.134	0.033	0.015	-0.104	0.109	-0.039	97.40	83.34	5.29	130.67	24.73
0.01	0.240	-0.575	0.632	-0.424	0.142	0.037	-0.009	-0.062	0.077	-0.029	97.97	83.16	5.31	130.39	24.56
0.02	0.258	-0.580	0.602	-0.410	0.147	0.020	0.061	-0.153	0.127	-0.040	98.33	87.35	5.32	128.71	24.20
0.01	0.260	-0.586	0.592	-0.379	0.129	0.015	0.084	-0.199	0.169	-0.053	97.22	86.60	5.34	126.98	23.79
0.01	0.253	-0.574	0.608	-0.422	0.151	0.024	0.047	-0.135	0.116	-0.036	98.60	87.13	5.32	124.65	23.44

0.09	0.291	-0.593	0.575	-0.409	0.161	0.038	0.046	-0.141	0.121	-0.040	98.31	87.50	5.31	123.00	23.16
0.11	0.312	-0.597	0.544	-0.392	0.164	0.040	0.072	-0.188	0.156	-0.051	98.15	89.35	5.30	121.70	22.95
0.06	0.289	-0.597	0.564	-0.375	0.141	0.033	0.071	-0.201	0.177	-0.058	98.38	88.96	5.32	120.44	22.65
0.06	0.261	-0.579	0.610	-0.433	0.159	0.047	-0.010	-0.064	0.068	-0.023	99.18	85.93	5.25	117.36	22.36
0.14	0.336	-0.602	0.513	-0.388	0.176	0.044	0.089	-0.209	0.155	-0.045	97.74	91.06	5.20	113.55	21.86
0.13	0.331	-0.601	0.519	-0.394	0.178	0.044	0.083	-0.201	0.148	-0.042	97.66	90.24	5.14	110.81	21.55
0.11	0.327	-0.594	0.519	-0.406	0.185	0.042	0.085	-0.200	0.142	-0.039	97.52	89.80	5.21	109.85	21.11
0.1	0.319	-0.591	0.539	-0.431	0.193	0.050	0.048	-0.144	0.101	-0.027	96.00	89.31	5.25	108.84	20.75
0.06	0.303	-0.470	0.258	-0.183	0.113	-0.022	0.318	-0.555	0.390	-0.110	78.09	77.42	5.31	107.38	20.23
0.97	0.297	0.316	-0.259	-0.460	-0.153	0.298	0.334	-0.265	-0.463	-0.156	44.11	37.52	5.27	106.35	20.19
0.87	0.267	0.451	0.410	0.204	0.047	0.202	0.486	0.446	0.193	0.014	77.05	92.80	5.25	107.76	20.54
0.98	0.474	0.410	-0.015	0.221	0.233	0.490	0.415	-0.042	0.222	0.202	70.22	75.87	5.24	110.55	21.11
0.97	0.126	0.165	0.339	0.523	0.264	0.106	0.149	0.333	0.538	0.254	86.31	91.25	5.31	112.76	21.24
0.96	0.112	-0.060	0.157	0.569	0.350	0.089	-0.068	0.137	0.609	0.333	80.83	79.50	5.40	112.38	20.81
0.97	0.109	0.096	0.292	0.553	0.294	0.092	0.081	0.281	0.570	0.287	84.18	86.75	5.48	109.61	20.03
0.97	0.116	0.122	0.315	0.540	0.280	0.095	0.102	0.306	0.562	0.272	84.25	86.81	5.51	105.83	19.22
0.97	0.126	0.167	0.344	0.517	0.261	0.103	0.143	0.335	0.541	0.256	84.25	89.75	5.51	102.21	18.56
0.94	0.516	-0.261	-0.521	-0.193	0.592	-0.007	0.018	0.025	0.026	0.065	13.92	-0.99	5.51	99.36	18.04
0.99	0.544	0.456	0.015	-0.480	-0.513	0.039	-0.016	0.008	-0.007	-0.001	78.62	6.50	5.52	97.30	17.61
0.97	0.453	0.005	-0.465	-0.025	0.194	0.486	0.024	-0.530	0.029	0.149	87.37	97.09	5.54	95.56	17.25
0.97	0.101	-0.287	0.266	-0.104	-0.404	0.241	-0.398	0.170	0.189	-0.617	64.46	71.25	5.55	93.92	16.93
0.99	0.192	0.094	0.049	0.033	0.061	0.554	0.580	0.083	-0.432	-0.333	19.40	85.95	5.55	92.08	16.59
0.95	0.544	0.433	0.042	-0.105	0.039	0.510	0.488	-0.008	-0.068	-0.004	92.27	94.30	5.55	90.38	16.28
0.79	0.444	0.407	0.238	0.271	0.141	0.257	0.479	0.356	0.220	0.131	86.02	93.08	5.57	88.81	15.96
0.98	0.034	-0.093	0.126	-0.148	-0.055	0.602	-0.311	0.132	0.125	-0.676	61.48	48.42	5.56	87.37	15.72
0.97	0.085	-0.205	0.263	-0.191	0.076	0.540	-0.566	0.111	0.300	-0.354	11.14	31.73	5.57	86.03	15.44
0.88	0.266	-0.475	0.446	-0.519	0.301	0.118	-0.250	0.232	-0.115	0.029	23.65	-23.27	5.56	84.41	15.19
0.81	0.425	0.414	0.269	0.261	0.134	0.259	0.476	0.366	0.217	0.120	88.60	91.94	5.57	82.88	14.88
0.83	0.493	0.317	0.377	0.147	0.092	0.308	0.466	0.364	0.200	0.023	90.58	96.60	5.55	81.07	14.61
0.82	0.542	0.274	0.353	0.169	0.088	0.330	0.460	0.324	0.209	0.037	92.44	95.89	5.52	79.32	14.38
0.92	0.453	0.350	-0.031	-0.329	-0.194	0.390	0.456	-0.048	-0.340	-0.221	86.11	90.29	5.42	77.07	14.20
0.85	0.690	0.095	0.230	-0.136	-0.083	0.438	0.431	0.122	-0.024	-0.210	91.48	93.91	5.32	74.70	14.05
0.86	0.673	0.129	0.168	-0.184	-0.114	0.443	0.433	0.089	-0.088	-0.239	91.51	94.95	5.22	72.45	13.87
0.86	0.684	0.113	0.147	-0.161	-0.120	0.458	0.427	0.062	-0.085	-0.232	93.31	94.73	5.17	71.00	13.72
0.87	0.651	0.188	0.127	-0.163	-0.128	0.454	0.454	0.072	-0.114	-0.226	92.20	96.92	5.19	70.67	13.63
0.85	0.697	0.104	0.218	-0.073	-0.065	0.454	0.441	0.114	0.011	-0.180	93.48	96.49	5.24	71.40	13.62
0.83	0.710	0.062	0.276	0.020	-0.006	0.430	0.432	0.144	0.113	-0.107	93.88	96.15	5.32	72.59	13.66
0.83	0.654	0.175	0.285	0.083	0.038	0.398	0.473	0.216	0.141	-0.050	93.65	98.93	5.37	73.47	13.68
0.83	0.681	0.118	0.293	0.051	0.019	0.414	0.452	0.186	0.132	-0.076	93.82	97.85	5.43	74.19	13.66
0.83	0.647	0.178	0.288	0.094	0.053	0.400	0.473	0.222	0.144	-0.037	93.90	98.25	5.47	74.48	13.61
0.92	0.438	0.398	0.077	-0.307	-0.188	0.373	0.482	0.070	-0.283	-0.241	88.02	91.40	5.49	74.47	13.56
0.83	0.709	0.035	0.302	0.007	0.001	0.429	0.418	0.146	0.117	-0.107	93.83	95.06	5.48	73.97	13.51
0.85	0.693	0.072	0.265	-0.116	-0.065	0.451	0.410	0.126	0.017	-0.195	91.35	92.50	5.46	73.13	13.40
0.75	0.449	-0.649	0.468	-0.047	-0.098	0.210	-0.068	-0.147	0.248	-0.126	89.79	78.14	5.46	72.25	13.25
0.85	0.702	0.087	0.250	-0.077	-0.064	0.445	0.427	0.119	0.037	-0.177	92.94	94.44	5.37	70.50	13.12
0.87	0.660	0.151	0.168	-0.188	-0.122	0.456	0.428	0.082	-0.094	-0.238	91.03	93.95	5.38	69.78	12.96
0.85	0.727	0.014	0.206	-0.089	-0.084	0.472	0.387	0.055	0.012	-0.194	94.63	93.22	5.37	68.82	12.83
0.92	0.450	0.374	0.016	-0.321	-0.196	0.378	0.468	0.011	-0.312	-0.239	89.67	92.75	5.39	68.25	12.67

0.9	0.532	0.282	0.075	-0.298	-0.197	0.421	0.434	0.039	-0.252	-0.273	89.85	90.74	5.25	65.71	12.52
0.88	0.644	0.074	0.029	-0.241	-0.214	0.480	0.347	-0.079	-0.190	-0.284	89.53	87.77	5.16	63.84	12.36
0.9	0.541	0.240	0.030	-0.298	-0.217	0.439	0.411	-0.022	-0.270	-0.279	91.10	92.90	5.13	62.61	12.20
0.91	0.481	0.300	0.016	-0.331	-0.219	0.406	0.426	-0.010	-0.313	-0.277	89.95	93.42	5.19	62.57	12.05
0.92	0.441	0.336	0.020	-0.338	-0.226	0.390	0.437	-0.007	-0.332	-0.269	90.31	93.62	5.22	62.01	11.87
0.92	0.450	0.340	0.026	-0.333	-0.214	0.391	0.443	0.007	-0.322	-0.267	89.88	91.73	5.23	60.96	11.66
0.92	0.456	0.329	0.025	-0.341	-0.212	0.393	0.435	0.007	-0.321	-0.273	90.74	92.73	5.20	59.60	11.47
0.92	0.469	0.310	0.018	-0.348	-0.216	0.399	0.422	-0.006	-0.319	-0.277	91.19	91.58	5.14	58.19	11.31
0.93	0.419	0.358	0.026	-0.358	-0.216	0.371	0.440	0.014	-0.340	-0.272	90.11	91.90	5.03	56.69	11.27
0.93	0.438	0.336	0.020	-0.351	-0.218	0.389	0.433	-0.005	-0.334	-0.272	92.78	93.27	4.91	55.18	11.24
0.93	0.456	0.309	0.008	-0.344	-0.229	0.407	0.419	-0.037	-0.328	-0.275	91.22	93.12	4.63	52.50	11.39
0.94	0.419	0.323	-0.040	-0.364	-0.233	0.390	0.414	-0.083	-0.366	-0.258	91.39	93.78	4.24	48.94	11.65
0.98	0.412	0.407	0.001	-0.309	-0.210	0.413	0.444	-0.026	-0.309	-0.248	90.74	96.56	3.71	44.44	12.09
0.96	0.342	0.268	-0.082	-0.436	-0.294	0.357	0.329	-0.139	-0.421	-0.310	86.12	90.11	3.35	41.43	12.45
0.91	0.580	0.200	-0.124	-0.250	-0.170	0.442	0.420	-0.156	-0.245	-0.247	91.64	93.60	3.12	39.70	12.74
0.9	0.603	0.123	-0.003	-0.293	-0.198	0.448	0.376	-0.085	-0.202	-0.327	89.72	91.67	3.04	39.25	12.92
0.96	0.353	0.277	-0.076	-0.426	-0.286	0.366	0.339	-0.127	-0.412	-0.309	90.52	92.18	2.97	38.80	13.05
0.9	0.558	0.219	-0.056	-0.297	-0.182	0.406	0.438	-0.073	-0.248	-0.305	91.61	91.84	2.92	38.34	13.14
0.91	0.570	0.206	-0.139	-0.244	-0.177	0.436	0.425	-0.171	-0.244	-0.250	89.41	91.29	2.86	37.84	13.24
0.98	0.375	0.393	0.006	-0.343	-0.240	0.385	0.430	-0.017	-0.344	-0.281	91.95	95.97	2.79	37.28	13.37
0.96	0.382	0.232	-0.102	-0.413	-0.294	0.401	0.302	-0.178	-0.390	-0.311	87.87	90.34	2.72	36.77	13.51
0.9	0.581	0.203	-0.086	-0.245	-0.170	0.429	0.447	-0.122	-0.221	-0.278	91.53	94.08	2.67	36.32	13.60
0.9	0.523	0.254	-0.041	-0.312	-0.187	0.379	0.460	-0.042	-0.261	-0.322	89.35	89.52	2.63	36.00	13.70
0.98	0.354	0.387	-0.040	-0.374	-0.230	0.369	0.423	-0.064	-0.381	-0.260	93.42	95.77	2.58	35.66	13.83
0.96	0.395	0.228	-0.159	-0.401	-0.261	0.409	0.303	-0.226	-0.391	-0.273	89.77	91.28	2.52	35.30	13.99
0.91	0.596	0.235	-0.133	-0.143	-0.129	0.465	0.467	-0.181	-0.187	-0.181	95.20	97.97	2.47	34.96	14.16
0.94	0.547	0.307	0.072	-0.186	-0.189	0.503	0.434	-0.025	-0.174	-0.242	95.65	94.98	2.44	34.85	14.26
0.77	0.564	-0.474	0.394	-0.399	0.081	0.284	0.122	-0.101	0.020	-0.175	93.37	92.85	2.46	35.33	14.34
0.76	0.523	-0.507	0.425	-0.417	0.090	0.259	0.076	-0.083	0.013	-0.162	92.87	92.69	2.51	36.62	14.57
0.95	0.435	0.357	0.006	-0.312	-0.240	0.418	0.429	-0.048	-0.313	-0.263	87.76	90.71	2.57	38.61	15.00
0.93	0.588	0.344	0.098	-0.129	-0.151	0.457	0.485	0.021	-0.102	-0.177	94.44	96.62	2.62	40.77	15.56
0.8	0.658	-0.272	0.344	-0.400	0.142	0.327	0.256	0.037	-0.054	-0.135	94.38	86.23	2.63	42.29	16.11
0.94	0.546	0.393	0.031	-0.143	-0.117	0.457	0.509	-0.022	-0.170	-0.126	94.52	96.81	2.61	42.99	16.52
0.97	0.360	0.438	-0.020	-0.364	-0.199	0.349	0.459	-0.045	-0.361	-0.204	88.98	93.00	2.54	42.98	16.94
0.82	0.683	-0.104	0.319	-0.338	0.125	0.360	0.358	0.096	-0.036	-0.152	93.78	81.92	2.49	42.77	17.19
0.95	0.477	0.470	0.121	-0.140	-0.110	0.417	0.533	0.081	-0.157	-0.126	93.59	94.63	2.44	42.46	17.46
0.8	0.676	-0.196	0.338	-0.369	0.179	0.340	0.291	0.098	-0.064	-0.091	96.28	85.57	2.42	42.32	17.47
0.8	0.676	-0.198	0.311	-0.386	0.176	0.341	0.293	0.082	-0.083	-0.104	95.49	85.38	2.42	42.20	17.44
0.93	0.464	0.490	0.148	-0.082	-0.081	0.357	0.571	0.169	-0.117	-0.122	94.57	95.43	2.40	41.58	17.35
0.88	0.582	0.080	0.066	-0.357	-0.189	0.344	0.422	-0.034	-0.163	-0.404	82.26	81.41	2.32	39.99	17.27
0.93	0.507	0.417	0.010	-0.166	-0.130	0.411	0.532	0.007	-0.213	-0.162	93.44	94.47	2.21	37.83	17.10
0.92	0.537	0.338	-0.073	-0.190	-0.151	0.425	0.502	-0.081	-0.234	-0.197	94.09	97.08	2.16	36.33	16.83
0.91	0.511	0.327	-0.044	-0.255	-0.178	0.377	0.501	-0.025	-0.255	-0.272	93.92	95.12	2.14	35.69	16.71
0.91	0.551	0.273	-0.123	-0.218	-0.173	0.408	0.479	-0.123	-0.251	-0.234	91.86	94.96	2.12	35.47	16.73
0.92	0.554	0.301	-0.137	-0.169	-0.139	0.441	0.484	-0.153	-0.239	-0.163	92.80	96.37	2.07	34.94	16.88
0.97	0.409	0.414	-0.018	-0.315	-0.181	0.413	0.455	-0.061	-0.324	-0.205	93.34	96.67	2.04	34.43	16.89
0.96	0.467	0.344	-0.071	-0.314	-0.185	0.454	0.407	-0.131	-0.310	-0.203	93.63	97.70	2.01	34.06	16.95
0.98	0.371	0.539	0.208	-0.120	-0.100	0.370	0.546	0.173	-0.147	-0.134	93.59	97.19	2.01	34.02	16.94

0.92	0.518	0.317	-0.134	-0.220	-0.165	0.409	0.486	-0.134	-0.274	-0.205	91.81	96.01	2.00	34.01	17.04
0.91	0.530	0.347	-0.007	-0.192	-0.155	0.396	0.528	-0.006	-0.207	-0.242	94.47	95.46	1.99	34.06	17.09
0.91	0.504	0.335	-0.032	-0.243	-0.181	0.371	0.514	-0.017	-0.245	-0.278	93.77	95.15	1.98	34.09	17.22
0.96	0.470	0.354	-0.068	-0.298	-0.172	0.458	0.420	-0.130	-0.302	-0.190	92.54	98.14	1.96	34.09	17.38
0.91	0.524	0.348	-0.017	-0.199	-0.164	0.388	0.529	-0.012	-0.214	-0.249	94.04	95.65	1.95	34.15	17.50
0.96	0.461	0.332	-0.109	-0.324	-0.174	0.448	0.400	-0.165	-0.326	-0.190	93.57	98.01	1.95	34.24	17.56
0.92	0.528	0.347	-0.087	-0.182	-0.147	0.418	0.513	-0.091	-0.242	-0.184	92.99	96.68	1.95	34.37	17.59
0.96	0.444	0.352	-0.109	-0.328	-0.169	0.428	0.418	-0.153	-0.340	-0.184	92.04	96.70	1.95	34.45	17.68
0.92	0.532	0.331	-0.107	-0.189	-0.156	0.418	0.501	-0.114	-0.247	-0.188	93.43	96.55	1.93	34.48	17.85
0.91	0.516	0.343	-0.021	-0.211	-0.170	0.381	0.527	-0.013	-0.225	-0.259	93.52	95.43	1.91	34.53	18.04
0.91	0.521	0.344	-0.017	-0.205	-0.181	0.378	0.527	-0.014	-0.212	-0.263	94.39	96.31	1.90	34.55	18.23
0.98	0.390	0.503	0.320	0.135	0.021	0.376	0.495	0.272	0.113	-0.025	92.91	98.33	1.88	34.61	18.43
0.91	0.493	0.343	-0.022	-0.242	-0.186	0.360	0.523	-0.003	-0.246	-0.287	93.46	94.48	1.86	34.66	18.59
0.92	0.512	0.353	-0.085	-0.208	-0.169	0.395	0.513	-0.079	-0.256	-0.210	92.75	96.02	1.86	34.71	18.69
0.91	0.517	0.357	-0.003	-0.193	-0.165	0.380	0.538	0.004	-0.209	-0.252	94.06	95.46	1.86	34.78	18.69
0.92	0.527	0.340	-0.102	-0.189	-0.162	0.410	0.507	-0.107	-0.247	-0.191	92.54	96.36	1.86	34.79	18.69
0.92	0.521	0.346	-0.100	-0.189	-0.154	0.409	0.513	-0.098	-0.253	-0.188	92.55	96.16	1.85	34.75	18.77
0.98	0.372	0.509	0.335	0.120	0.008	0.359	0.501	0.292	0.097	-0.038	92.15	98.86	1.83	34.66	18.91
0.92	0.509	0.384	-0.040	-0.178	-0.151	0.396	0.536	-0.033	-0.231	-0.197	93.87	95.42	1.81	34.53	19.05
0.91	0.504	0.347	-0.034	-0.214	-0.176	0.372	0.532	-0.018	-0.236	-0.266	93.40	96.02	1.80	34.42	19.09
0.91	0.526	0.333	-0.031	-0.197	-0.182	0.383	0.527	-0.034	-0.212	-0.261	93.70	96.50	1.79	34.26	19.16
0.91	0.517	0.339	-0.052	-0.198	-0.168	0.385	0.531	-0.042	-0.233	-0.248	93.50	96.55	1.77	34.21	19.28
0.91	0.533	0.327	-0.046	-0.181	-0.168	0.399	0.528	-0.052	-0.215	-0.241	93.95	97.02	1.76	34.14	19.38
0.91	0.529	0.339	-0.019	-0.178	-0.172	0.391	0.536	-0.027	-0.201	-0.250	94.12	96.24	1.74	34.03	19.54
0.88	0.646	0.180	0.029	-0.070	-0.124	0.433	0.522	-0.082	-0.032	-0.249	95.03	97.85	1.73	33.79	19.58
0.89	0.574	0.242	0.026	-0.162	-0.174	0.394	0.533	-0.042	-0.112	-0.318	93.92	95.19	1.71	33.51	19.60
0.92	0.489	0.412	0.006	-0.158	-0.142	0.383	0.560	0.016	-0.213	-0.201	93.83	95.04	1.71	33.41	19.56
0.87	0.643	0.083	0.050	-0.140	-0.145	0.417	0.490	-0.119	-0.018	-0.330	95.23	97.08	1.71	33.43	19.58
0.89	0.582	0.223	-0.010	-0.147	-0.185	0.396	0.529	-0.085	-0.106	-0.318	94.50	97.32	1.70	33.51	19.78
0.89	0.595	0.287	0.027	-0.066	-0.128	0.409	0.561	-0.028	-0.067	-0.233	93.23	97.95	1.69	33.56	19.88
0.83	0.692	-0.208	0.222	-0.168	-0.028	0.397	0.360	-0.155	0.125	-0.269	94.69	96.58	1.68	33.52	20.00
0.85	0.701	0.023	0.100	-0.011	-0.055	0.406	0.500	-0.135	0.127	-0.215	96.00	97.64	1.68	33.55	19.95
0.84	0.711	-0.098	0.140	-0.068	-0.044	0.409	0.437	-0.163	0.131	-0.237	95.91	97.38	1.67	33.48	20.07
0.84	0.701	-0.086	0.155	-0.119	-0.044	0.408	0.439	-0.142	0.106	-0.266	95.60	97.43	1.66	33.52	20.16
0.87	0.634	0.133	0.021	-0.127	-0.126	0.418	0.516	-0.103	-0.044	-0.306	93.81	98.40	1.66	33.56	20.27
0.84	0.697	-0.100	0.123	-0.105	-0.062	0.402	0.438	-0.179	0.113	-0.277	95.97	97.46	1.66	33.73	20.29
0.87	0.644	0.183	0.032	-0.057	-0.096	0.415	0.547	-0.073	-0.007	-0.247	93.61	98.81	1.66	33.84	20.40
0.83	0.705	-0.162	0.165	-0.130	-0.026	0.398	0.404	-0.170	0.121	-0.257	95.83	97.90	1.66	33.99	20.49
0.88	0.595	0.214	-0.027	-0.104	-0.158	0.393	0.550	-0.102	-0.072	-0.302	93.97	98.78	1.65	34.17	20.67
0.87	0.629	0.203	0.014	-0.060	-0.105	0.406	0.558	-0.077	-0.017	-0.258	93.07	99.05	1.66	34.47	20.78
0.86	0.648	0.102	0.027	-0.113	-0.110	0.411	0.518	-0.119	-0.006	-0.305	93.50	98.86	1.67	34.73	20.85
0.85	0.661	0.043	-0.003	-0.049	-0.110	0.393	0.514	-0.198	0.072	-0.291	95.10	97.88	1.67	34.97	20.95
0.86	0.641	0.074	-0.026	-0.088	-0.142	0.403	0.508	-0.182	0.003	-0.318	94.11	97.86	1.67	35.15	21.03
0.87	0.602	0.196	-0.026	-0.107	-0.141	0.393	0.551	-0.105	-0.059	-0.307	92.16	98.58	1.68	35.48	21.16
0.87	0.600	0.205	-0.037	-0.090	-0.142	0.392	0.557	-0.111	-0.055	-0.300	91.67	98.82	1.68	35.86	21.31
0.97	0.502	-0.169	-0.662	-0.165	0.504	0.007	-0.008	-0.001	-0.006	0.017	23.76	-47.79	1.70	36.32	21.39
0.98	0.175	-0.173	0.259	-0.153	0.167	0.699	-0.503	0.260	-0.111	0.002	86.66	-52.66	1.70	36.64	21.58
0.86	0.624	0.165	0.005	-0.097	-0.112	0.405	0.547	-0.093	-0.031	-0.298	91.32	98.79	1.71	36.86	21.54

0.86	0.620	0.195	-0.036	-0.015	-0.118	0.382	0.574	-0.128	0.020	-0.263	92.18	99.09	1.71	37.00	21.67
0.87	0.600	0.244	-0.022	-0.071	-0.122	0.391	0.571	-0.069	-0.059	-0.268	90.94	98.72	1.73	37.19	21.56
0.85	0.642	0.188	0.018	-0.023	-0.071	0.381	0.578	-0.080	0.047	-0.243	90.93	98.85	1.73	37.46	21.69
0.86	0.619	0.201	0.008	-0.089	-0.104	0.401	0.558	-0.062	-0.039	-0.282	90.98	98.25	1.74	37.81	21.69
0.86	0.611	0.247	0.034	-0.063	-0.081	0.389	0.581	-0.019	-0.018	-0.254	90.14	98.50	1.75	38.23	21.87
0.86	0.607	0.258	0.056	-0.081	-0.070	0.393	0.577	0.013	-0.033	-0.251	90.76	98.23	1.77	38.71	21.82
0.85	0.629	0.240	0.104	-0.077	-0.021	0.393	0.570	0.051	-0.001	-0.218	90.08	98.36	1.79	39.20	21.93
0.86	0.596	0.288	0.065	-0.051	-0.068	0.380	0.591	0.033	-0.014	-0.236	90.34	98.35	1.81	39.73	21.91
0.85	0.621	0.246	0.098	-0.080	-0.034	0.392	0.572	0.051	-0.007	-0.232	88.18	97.93	1.83	40.24	22.04
0.85	0.609	0.291	0.109	-0.003	-0.019	0.365	0.598	0.071	0.051	-0.183	90.16	99.26	1.84	40.70	22.08
0.85	0.595	0.311	0.143	-0.028	0.000	0.366	0.590	0.123	0.031	-0.175	90.61	98.92	1.86	41.19	22.19
0.85	0.593	0.310	0.157	-0.044	0.008	0.373	0.579	0.143	0.015	-0.173	90.78	97.94	1.87	41.68	22.33
0.86	0.586	0.305	0.103	-0.060	-0.057	0.388	0.581	0.087	-0.030	-0.223	88.86	97.85	1.89	42.29	22.36
0.85	0.562	0.359	0.178	0.008	0.028	0.341	0.594	0.184	0.053	-0.132	91.06	97.93	1.91	42.81	22.47
0.85	0.548	0.366	0.209	-0.012	0.041	0.339	0.582	0.222	0.043	-0.127	92.47	95.05	1.92	43.29	22.58
0.86	0.546	0.376	0.152	0.003	-0.018	0.352	0.600	0.165	0.019	-0.161	89.43	99.31	1.92	43.73	22.78
0.85	0.587	0.315	0.161	-0.022	-0.007	0.369	0.584	0.144	0.030	-0.176	88.12	98.56	1.93	44.07	22.80
0.86	0.577	0.324	0.108	-0.022	-0.061	0.379	0.592	0.095	-0.007	-0.206	87.46	98.07	1.95	44.26	22.70
0.86	0.589	0.300	0.099	-0.039	-0.068	0.394	0.581	0.078	-0.023	-0.219	87.72	97.59	1.95	44.20	22.66
0.86	0.583	0.314	0.091	-0.021	-0.068	0.385	0.591	0.075	-0.012	-0.211	87.95	98.07	1.94	44.10	22.68
0.86	0.559	0.353	0.134	-0.008	-0.036	0.365	0.599	0.135	0.007	-0.183	87.94	98.60	1.94	44.01	22.66
0.86	0.546	0.373	0.152	0.014	-0.024	0.351	0.602	0.159	0.028	-0.163	88.13	99.09	1.96	43.99	22.42
0.86	0.528	0.386	0.191	-0.003	0.001	0.346	0.590	0.210	0.021	-0.150	89.48	97.93	1.98	44.01	22.19
0.86	0.551	0.360	0.156	-0.011	-0.024	0.364	0.594	0.160	0.009	-0.175	87.90	98.61	1.99	44.03	22.09
0.86	0.545	0.363	0.170	-0.023	-0.019	0.363	0.589	0.179	0.002	-0.176	87.92	97.44	1.99	44.15	22.20
0.85	0.564	0.340	0.186	-0.018	0.008	0.358	0.585	0.183	0.033	-0.162	88.11	97.36	1.99	44.34	22.32
0.86	0.526	0.390	0.186	0.020	-0.007	0.342	0.597	0.202	0.035	-0.146	89.05	99.16	1.99	44.57	22.36
0.86	0.535	0.374	0.180	-0.009	-0.018	0.357	0.591	0.191	0.011	-0.168	87.20	97.79	2.01	44.86	22.27
0.85	0.505	0.406	0.227	0.042	0.048	0.308	0.590	0.258	0.078	-0.097	91.81	96.28	2.03	45.10	22.22
0.86	0.500	0.405	0.228	0.014	0.011	0.331	0.584	0.253	0.038	-0.134	88.19	95.64	2.05	45.41	22.19
0.86	0.521	0.399	0.169	0.042	-0.018	0.336	0.607	0.189	0.042	-0.143	87.53	98.84	2.06	45.70	22.21
0.86	0.491	0.418	0.222	0.041	0.014	0.321	0.591	0.253	0.053	-0.117	89.57	98.21	2.07	46.00	22.22
0.86	0.517	0.393	0.192	0.018	-0.014	0.344	0.596	0.209	0.029	-0.151	87.02	98.75	2.08	46.24	22.25
0.85	0.462	0.434	0.264	0.055	0.075	0.282	0.574	0.315	0.089	-0.063	93.60	92.42	2.08	46.37	22.30
0.86	0.495	0.411	0.221	0.033	0.004	0.326	0.592	0.245	0.049	-0.132	86.96	97.48	2.08	46.48	22.31
0.86	0.425	0.458	0.280	0.080	0.065	0.271	0.567	0.337	0.092	-0.053	93.76	93.31	2.08	46.51	22.31
0.87	0.481	0.434	0.194	0.048	-0.025	0.325	0.605	0.223	0.031	-0.134	86.32	98.06	2.07	46.01	22.22
0.86	0.509	0.396	0.210	0.012	-0.002	0.344	0.588	0.231	0.025	-0.145	87.75	97.89	2.04	45.10	22.06
0.87	0.571	0.301	0.046	-0.044	-0.112	0.395	0.593	0.015	-0.068	-0.233	86.50	97.80	2.02	44.11	21.86
0.86	0.473	0.432	0.233	0.062	0.028	0.299	0.596	0.271	0.065	-0.095	90.79	98.22	2.03	44.26	21.79
0.86	0.462	0.433	0.252	0.065	0.023	0.298	0.589	0.284	0.071	-0.095	88.37	97.91	2.06	45.32	22.01
0.86	0.423	0.451	0.287	0.086	0.045	0.274	0.570	0.336	0.091	-0.068	91.83	95.58	2.08	46.70	22.40
0.87	0.428	0.450	0.280	0.083	0.010	0.294	0.577	0.312	0.069	-0.086	88.16	98.53	2.08	47.48	22.82
0.86	0.437	0.442	0.277	0.090	0.034	0.288	0.575	0.319	0.085	-0.074	89.74	97.66	2.05	47.48	23.15
0.86	0.433	0.442	0.280	0.090	0.037	0.285	0.576	0.321	0.089	-0.073	90.27	97.20	2.01	46.90	23.35
0.86	0.511	0.386	0.220	0.046	-0.010	0.346	0.591	0.226	0.040	-0.129	87.32	98.65	1.97	45.95	23.32
0.86	0.488	0.404	0.246	0.050	0.017	0.329	0.585	0.265	0.052	-0.111	89.15	98.13	1.95	44.87	22.95
0.85	0.508	0.385	0.242	0.038	0.041	0.326	0.585	0.260	0.064	-0.107	91.71	96.26	1.94	43.77	22.57

0.85	0.491	0.409	0.231	0.060	0.053	0.306	0.596	0.264	0.078	-0.087	91.17	96.62	1.93	42.75	22.21
0.85	0.513	0.386	0.230	0.039	0.050	0.326	0.591	0.251	0.064	-0.099	92.94	95.89	1.90	41.84	21.97
0.86	0.476	0.423	0.235	0.044	0.038	0.316	0.592	0.273	0.049	-0.100	92.70	96.23	1.90	41.18	21.68
0.86	0.512	0.398	0.187	0.044	0.010	0.337	0.608	0.205	0.043	-0.124	89.76	99.53	1.91	40.72	21.39
0.83	0.635	-0.058	-0.058	0.055	-0.160	0.399	0.455	-0.308	0.130	-0.289	91.01	89.13	1.90	40.54	21.30
0.84	0.629	0.203	0.138	-0.022	-0.030	0.424	0.561	0.039	0.045	-0.210	89.04	98.35	1.92	40.61	21.15
0.86	0.532	0.363	0.170	-0.001	-0.023	0.376	0.598	0.165	0.005	-0.173	89.17	98.58	1.92	40.92	21.31
0.86	0.501	0.395	0.214	0.020	0.009	0.349	0.595	0.228	0.029	-0.135	91.12	98.10	1.95	41.50	21.32
0.86	0.503	0.401	0.193	0.048	-0.001	0.342	0.607	0.205	0.044	-0.129	89.42	99.48	1.96	42.14	21.50
0.86	0.486	0.413	0.215	0.047	0.005	0.332	0.602	0.233	0.048	-0.125	88.71	99.09	1.99	42.90	21.55
0.84	0.632	0.196	0.091	0.024	-0.067	0.410	0.575	-0.017	0.063	-0.214	89.94	98.48	2.01	43.56	21.71
0.84	0.632	0.196	0.111	-0.007	-0.066	0.413	0.566	0.005	0.041	-0.229	87.29	98.47	2.02	44.16	21.92
0.86	0.504	0.400	0.204	0.037	-0.010	0.346	0.598	0.212	0.026	-0.139	88.15	99.00	2.03	44.60	21.97
0.87	0.565	0.260	0.044	-0.095	-0.147	0.434	0.551	-0.011	-0.121	-0.271	83.85	96.33	2.03	44.77	22.04
0.85	0.501	0.395	0.229	0.041	0.025	0.327	0.595	0.245	0.060	-0.118	90.91	97.08	2.03	44.86	22.12
0.85	0.470	0.425	0.240	0.070	0.047	0.296	0.598	0.274	0.083	-0.086	91.79	96.51	2.01	44.85	22.29
0.87	0.407	0.468	0.275	0.092	0.024	0.280	0.583	0.317	0.075	-0.079	88.59	98.49	2.01	44.84	22.28
0.85	0.521	0.372	0.225	0.023	0.016	0.348	0.588	0.227	0.045	-0.135	89.56	97.98	2.03	44.67	22.03
0.86	0.500	0.398	0.212	0.039	-0.007	0.344	0.599	0.219	0.037	-0.137	87.95	98.57	2.03	44.40	21.88
0.85	0.521	0.374	0.217	0.024	0.018	0.346	0.593	0.220	0.046	-0.134	91.21	97.71	2.03	44.23	21.82
0.85	0.473	0.432	0.215	0.073	0.046	0.299	0.609	0.252	0.074	-0.084	90.36	97.74	2.02	44.25	21.91
0.85	0.534	0.353	0.214	0.005	0.000	0.362	0.589	0.199	0.038	-0.160	87.66	97.46	2.04	44.49	21.79
0.86	0.423	0.460	0.261	0.085	0.048	0.280	0.589	0.308	0.078	-0.070	92.22	96.28	2.06	44.67	21.69
0.61	0.318	-0.586	0.596	-0.362	0.091	0.136	-0.059	-0.065	0.150	-0.110	72.43	55.16	2.07	44.84	21.63
0.83	0.604	0.262	0.178	-0.008	0.017	0.382	0.586	0.110	0.063	-0.171	90.86	98.96	2.07	45.00	21.70
0.83	0.564	0.338	0.132	0.054	0.023	0.334	0.630	0.108	0.086	-0.138	90.63	99.61	2.07	45.24	21.81
0.84	0.570	0.325	0.149	0.041	-0.007	0.361	0.611	0.116	0.064	-0.156	89.40	99.21	2.09	45.51	21.81
0.85	0.514	0.394	0.193	0.056	0.012	0.334	0.609	0.202	0.058	-0.121	89.63	99.57	2.09	45.71	21.86
0.85	0.480	0.421	0.223	0.064	0.033	0.308	0.604	0.249	0.071	-0.101	91.17	98.39	2.09	45.84	21.94
0.85	0.473	0.422	0.238	0.053	0.042	0.305	0.597	0.268	0.066	-0.099	92.12	96.07	2.09	45.89	21.98
0.98	0.177	0.600	0.251	-0.563	-0.478	-0.007	0.007	-0.001	-0.011	0.008	26.46	-18.49	2.09	45.87	21.99
0.99	0.324	0.439	0.265	0.044	0.017	0.531	0.536	-0.103	-0.128	0.185	41.37	-1.29	2.10	45.85	21.87
0.81	0.609	0.257	0.096	0.039	0.053	0.329	0.640	0.023	0.119	-0.130	90.39	98.66	2.09	45.65	21.91
0.84	0.521	0.387	0.193	0.048	0.035	0.320	0.614	0.198	0.080	-0.114	90.41	97.89	2.09	45.50	21.78
0.85	0.512	0.400	0.179	0.051	0.007	0.335	0.613	0.191	0.053	-0.128	88.42	99.53	2.09	45.31	21.70
0.85	0.465	0.434	0.238	0.051	0.047	0.301	0.597	0.273	0.067	-0.092	92.71	95.45	2.10	45.41	21.61
0.84	0.532	0.367	0.210	0.015	0.034	0.339	0.600	0.205	0.062	-0.130	92.34	96.37	2.09	45.05	21.61
0.84	0.545	0.348	0.208	0.028	0.025	0.347	0.599	0.184	0.077	-0.135	88.82	98.10	2.06	44.44	21.59
0.86	0.597	0.190	-0.100	0.089	-0.163	0.366	0.577	-0.209	0.052	-0.223	79.22	94.14	2.04	43.58	21.38
0.85	0.517	0.397	0.201	0.031	0.031	0.307	0.609	0.217	0.072	-0.124	86.15	96.90	2.04	43.33	21.20
0.88	0.371	0.489	0.302	0.104	0.023	0.246	0.570	0.346	0.097	-0.070	86.54	96.59	2.06	43.52	21.08
0.87	0.592	0.195	-0.117	0.029	-0.184	0.409	0.542	-0.213	-0.026	-0.238	84.29	93.56	2.08	43.90	21.11
0.85	0.532	0.380	0.167	0.034	0.005	0.344	0.612	0.168	0.051	-0.141	88.64	99.68	2.11	44.54	21.13
0.83	0.535	0.338	-0.052	0.172	-0.029	0.310	0.654	-0.088	0.143	-0.124	85.74	94.72	2.16	45.31	20.99
0.86	0.451	0.445	0.241	0.049	0.026	0.313	0.594	0.271	0.048	-0.103	91.21	97.05	2.24	46.35	20.69